

Article

Impact of Urbanization on Urban Heat Island Intensity in Major Districts of Bangladesh Using Remote Sensing and Geo-Spatial Tools

Md. Naimur Rahman ^{1,*}, Md. Rakib Hasan Rony ¹, Farhana Akter Jannat ¹, Subodh Chandra Pal ²,
Md. Saiful Islam ³, Edris Alam ^{4,5} and Abu Reza Md. Towfiqul Islam ^{6,*}

¹ Department of Geography and Environmental Science, Begum Rokeya University, Rangpur 5400, Bangladesh; rakib.h.ronie@gmail.com (M.R.H.R.); farhana01jannat@gmail.com (F.A.J.)

² Department of Geography, The University of Burdwan, Bardhaman 713104, India; scpal@geo.buruniv.ac.in

³ Department of Soil Science, Patuakhali Science and Technology University, Dumki, Patuakhali 8602, Bangladesh; saiful@pstu.ac.bd

⁴ Faculty of Resilience, Rabdan Academy, Abu Dhabi 22401, United Arab Emirates; ealam@ra.ac.ae

⁵ Department of Geography and Environmental Studies, University of Chittagong, Chittagong 4331, Bangladesh

⁶ Department of Disaster Management, Begum Rokeya University, Rangpur 5400, Bangladesh

* Correspondence: naimurbrur@gmail.com (M.N.R.); towfiq_dm@brur.ac.bd (A.R.M.T.I.)

Abstract: Urbanization is closely associated with land use land cover (LULC) changes that correspond to land surface temperature (LST) variation and urban heat island (UHI) intensity. Major districts of Bangladesh have a large population base and commonly lack the resources to manage fast urbanization effects, so any rise in urban temperature influences the population both directly and indirectly. However, little is known about the impact of rapid urbanization on UHI intensity variations during the winter dry period in the major districts of Bangladesh. To this end, we aim to quantify spatiotemporal associations of UHI intensity during the winter period between 2000 and 2019 using remote-sensing and geo-spatial tools. Landsat-8 and Landsat-5 imageries of these major districts during the dry winter period from 2000 to 2020 were used for this purpose, with overall precision varying from 81% to 93%. The results of LULC classification and LST estimation showed the existence of multiple UHIs in all major districts, which showed upward trends, except for the Rajshahi and Rangpur districts. A substantial increase in urban expansion was observed in Barisal > 32%, Mymensingh > 18%, Dhaka > 17%, Chattogram > 14%, and Rangpur > 13%, while a significant decrease in built-up areas was noticed in Sylhet < -1.45% and Rajshahi < -3.72%. We found that large districts have greater UHIs than small districts. High UHI intensities were observed in Mymensingh > 10 °C, Chattogram > 9 °C, and Barisal > 8 °C compared to other districts due to dense population and unplanned urbanization. We identified higher LST (hotspots) zones in all districts to be increased with the urban expansion and bare land. The suburbanized strategy should prioritize the restraint of the high intensity of UHIs. A heterogeneous increase in UHI intensity over all seven districts was found, which might have potential implications for regional climate change. Our study findings will enable policymakers to reduce UHI and the climate change effect in the concerned districts.

Keywords: LULC; LST; UHI; Bangladesh; climate; urbanization



Citation: Rahman, M.N.; Rony, M.R.H.; Jannat, F.A.; Chandra Pal, S.; Islam, M.S.; Alam, E.; Islam, A.R.M.T. Impact of Urbanization on Urban Heat Island Intensity in Major Districts of Bangladesh Using Remote Sensing and Geo-Spatial Tools. *Climate* **2022**, *10*, 3. <https://doi.org/10.3390/cli10010003>

Academic Editor: Forrest M. Hoffman

Received: 29 October 2021

Accepted: 2 December 2021

Published: 4 January 2022

Publisher's Note: MDPI stays neutral with regard to jurisdictional claims in published maps and institutional affiliations.



Copyright: © 2022 by the authors. Licensee MDPI, Basel, Switzerland. This article is an open access article distributed under the terms and conditions of the Creative Commons Attribution (CC BY) license (<https://creativecommons.org/licenses/by/4.0/>).

1. Introduction

Urbanization, for instance, in the form of roads, industries, buildings, etc., contributes significantly to changing climatic measures by warming the atmosphere and generating carbon emissions associated with increased surface temperature, referred to as an urban heat island (UHI) [1]. It involves population migration, socioeconomic changes, physical diversion, and multiple differentiations in land surface observation [2]. The urban heat

island (UHI) intensity has an upward trend, creating exceptions to challenges as the world's urban population raised 55.715% in 2019, expected to increase to 68% by 2050 [3]. Dynamic temperature increase is observed in structurally compact developed areas, which causes the enhancement of UHI in urban areas compared with rural areas [4]. Several previous investigations indicated the voluminous propagation of heat due to building form, land use pattern and industrialization, which results in an increase in land surface temperature (LST) in urban and suburban areas [5–9]. Structural urban expansion, population increase, and other anthropogenic constructions cause UHI extension, impacting the local climate by reducing precipitation, evapotranspiration, and air and water quality, which negatively affects human health and living conditions [9,10]. Thus, UHIs have recently become a topic of interest among many research scholars.

The delineation of the urban climatic phenomenon and LST mutation have been illustrated through diverse approaches that may be demonstrated through earth and satellite observations. Earth observation, which relies on ground assessment, depends on station-wise analyses for the exposition of atmospheric temperature contraposition as the value of UHI predominance [11,12]. However, several previous studies demonstrated substantial repercussions on satellite-based observation systems for LST retrieval in the spatiotemporal measures of UHI intensity [13,14]. Furthermore, earlier investigations, using geometrical resolution-based data, have reported multi-nonlinear regression for the prediction of UHIs. Night satellite images for local-scale UHI extraction, conventional measurements for the spatiotemporal UHI model, and moderate-scale synoptic data were assessed for UHI observations [15–17]. Another exploration was based on 75 different studies of UHI exhibiting MODIS (28%), Landsat TM (54%), and ETM (34%) utilization [18]. It has become more common to investigate spatiotemporal UHI differentiations and LST changes using the thermal approach of remote sensing [18].

The UHI concept was first introduced in 1818, while its importance gained acknowledgement after the 1970s [19,20]. Earlier findings elucidated that TIR imageries, or Landsat imageries, are vital for UHI intensity calculation [21]. LULC and normalized difference vegetation index (NDVI) differentiation are adopted to identify UHI intensities [22]. A large number of studies have been performed to assess the spatiotemporal association between LST and vegetation change in estimating UHI intensity in various urban areas worldwide [23–26]. In addition, the pattern of LULC types is easily identified due to rapid urbanization and high residential growth, while seasonal variations in vegetation and analyzing urban regions employing variations in LULC types from undeveloped to developed types have been complicated. Various remotely sensed indexes, namely the soil-adjusted vegetation index, normalized difference building index, and normalized difference drought index, are insufficient in built-up and barren land observations [27–29]. This problem results from the difficulty in pixel couplings for the spectral response to heterogeneous LULC types, such as water bodies, vegetation, barren land, and built-up lands [30]. A coupling index of LULC, LST, and UHI was employed in this research to overcome this difficulty.

Bangladesh, a low-lying deltaic nation, with an overall population of 162 million and a density of 1120 km² [31], is one of the most susceptible nations to climate change [32]. It consists of 8 administration divisions, 64 districts/cites, and 12 city corporations. Four diverse seasons, i.e., winter (December–February), pre-monsoon (March–May), monsoon (June–September), and post-monsoon (October–November), prevail in the country. The country experiences a distinct cold and dry climatic condition during the winter period, with a warm, humid pre-monsoon and a rainy monsoon period and notable seasonality in precipitation and surface temperature. Because of the high population growth and urban expansion, the country experiences a noteworthy reduction in land surface (agricultural and vegetation land) and a related expansion of urban land surface [33]. For instance, the nation's urban population increased from 22.5 million in 1990 to 60 million in 2019 [31]. In addition, the trend of high surface temperature is predicted to rise, and a dry spell winter period may become evident [34,35]. Besides, the country is highly affected by extreme

events such as drought and floods. Thus, policy intervention and resilience to lessen the effect of these extreme phenomena are well documented. Rapid urbanization and urban warming are a matter of concern in recent times due to their negative effects on major urban districts [36]. Therefore, a comprehensive study on the impacts of urbanization on UHI intensity is urgently required for a highly populous, resource-limited and poor vulnerable country such as Bangladesh.

Although the effect of LULC changes on LST has been thoroughly investigated by several research scholars in Bangladeshi cities [32,35], only two have explored UHI intensity at the seasonal scale over large Bangladeshi cities [37,38]. For example, [39] used MODIS datasets from 2002 to 2014 during the monsoon period (June–September) to assess UHI intensity across megacities of Asian countries such as Dhaka [36]. Dewan focused on daily and seasonal surface UHI spatiotemporal trends and probable drivers in five cities of Bangladesh. Another recent study performed by Dewan [36] utilized a diurnal (day/night) MODIS time-series dataset from 2000–2019 to determine surface UHI, driver and variability in the similar five cities of Bangladesh. These previously cited studies improved our understanding of spatial and temporal changes of LST and associated UHI; however, these studies have adopted limited datasets (e.g., selected years) and are restricted in scope (e.g., single city or multiple cities). These earlier works also investigated the nexus between LST and vegetation, but the impact of urbanization on major districts' regional climate by appraising the presence of UHI intensity has not yet been performed with regard to the major districts of Bangladesh. The critical literature survey indicates that reference datasets about the UHI intensity of the country's districts are lacking, except for the recent studies [36]. However, a thorough and recent analysis of UHI in association with LST during the dry winter period has not been carried out using high-resolution imageries in major districts of Bangladesh. Our hypothesis is that the impact of urbanization on UHI intensity over major districts in the seven climatic regions varies between these districts, even if they are in the same nation [40]. Therefore, the preliminary intention of this research is to generate reference datasets on spatial and temporal changes of UHI intensity in the seven major districts of the country using high-resolution satellite images data. Seven major districts, namely Dhaka, Chattergram, Sylhet, Mymensingh, Rangpur, Barishal, and Rajshahi, were chosen based on urban expansion, population size, important divisional cities, and the accessibility of supplementary information [31,41]. The main goals are to (i) examine spatiotemporal associations of UHI intensity during the winter period between 2000 and 2019; (ii) determine the significance of urban LULC expansion in the variation of UHI intensity and LST patterns in seven major districts of Bangladesh. The outcomes of this work can be of value in building region-specific adaptation policies to lessen environmental effects associated with urbanization-derived LST warming and to enhance the quality of life of urban residents.

2. Data and Methods

Landsat-5 and Landsat-8 satellite images were downloaded from (<https://earthexplorer.usgs.gov/>; accessed on 20 February 2021) for the years 2000, 2010, and 2020 according to specific paths and rows for the study area purposes during the winter time. There are some reasons for selecting the research data, i.e., during the winter period between 2000 and 2019. The first reason is that satellite observation in wintertime greatly influences UHI intensity owing to the fact that the overpass time varies between districts. The second reason is that energy and health effects vary between summer and winter, so characterizing the winter seasonal scale of the local climate is determined as crucial. The third reason is that measures undertaken to curb urban warming may intensify UHI intensity in wintertime [38]. As for calculating LST, NDVI, and LULC classification, the images were preprocessed and analyzed in ArcGIS 10.8. The following flowchart represents the process of this study (Figure 1).

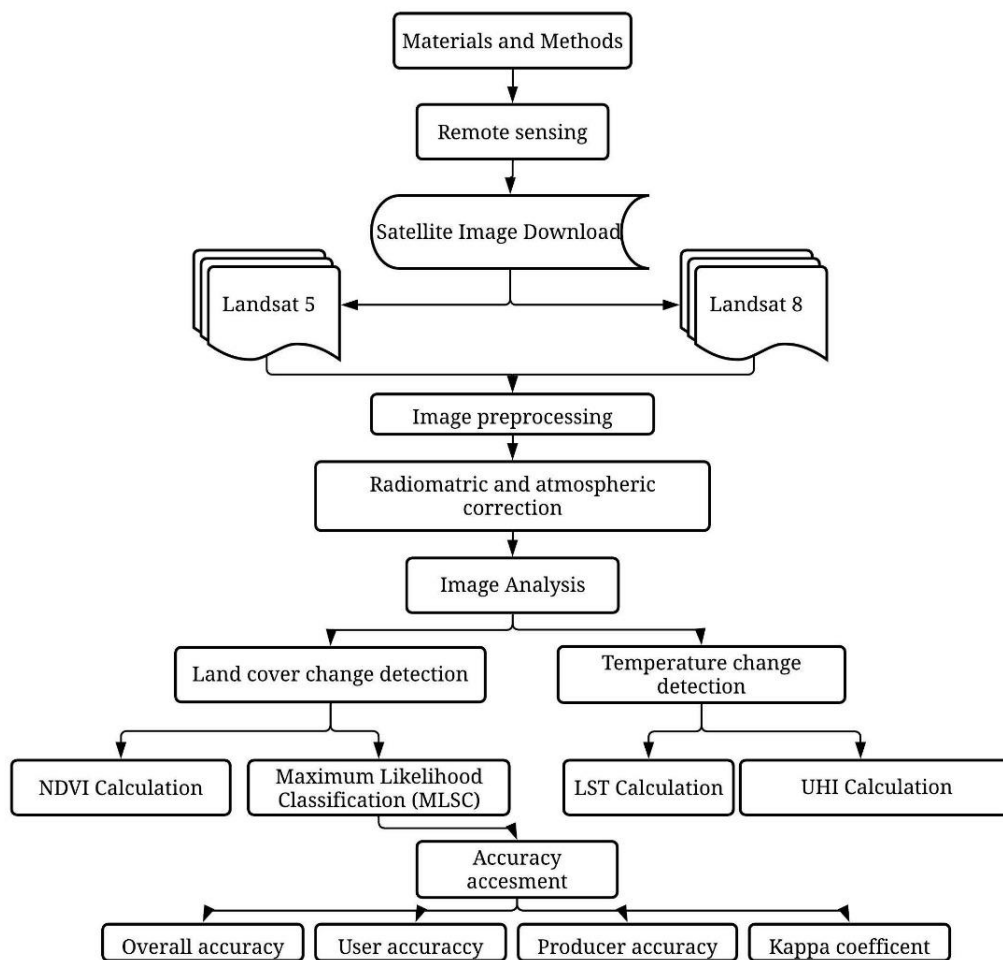


Figure 1. Methodological flowchart of the study area.

2.1. Study Area

The study area contained seven major urban districts in six existing climatic zones, namely Barisal (south-eastern zone), Chattogram (south-eastern zone), Dhaka (south-central zone), Mymensingh (south-central zone), Rajshahi (western climatic zone), Rangpur (northern part of the northern region), and Sylhet (north-eastern zone) [42]. The annual average temperature ranges from 35.1 °C to 12.1 °C, 32.5 °C to 13.5 °C, 34.5 °C to 11.5 °C, 33.3 °C and 12 °C, 37.8 °C to 11.2 °C, 32.3 °C to 11.2 °C, and 33.2 °C to 13.6 °C for Barisal, Chattogram, Dhaka, Mymensingh, Rajshahi, Rangpur, and Sylhet, respectively [31]. Furthermore, precipitation variation prevails as 1955 mm, 3378 mm, 1931 mm, 2174 mm, 1862 mm, 2931 mm, 3334 mm for Barisal, Chattogram, Dhaka, Mymensingh, Rajshahi, Rangpur, and Sylhet, accordingly [31]. The elevation pattern was found to be high in Chattogram and Sylhet, ranging from 328 to 293 m (Figures 2 and 3). Population [43], approximate district area [31], and climatic condition [35,44] are demonstrated for the years 2000, 2010, and 2020 (Table 1).

Table 1. Different characteristics of study area.

District	Year	Population	Area (sq. km)	Climate	District	Year	Population	Area (sq. km)	Climate	
Barisal	2000	248,000	2785.52	Tropical savanna	Chattogram	2000	3,308,000	5282.92	Tropical monsoon	
	2010	344,000				2010	4,106,000			
	2020	484,000				2020	5,020,000			
Dhaka	2000	10,285,000	1497.17	Tropical savanna	Mymensingh	2000	350,000	4394.57	Tropical monsoon	
	2010	14,731,000				2010	401,000			
	2020	21,006,000				2020	460,000			
Rajshahi	2000	678,000	2401	Tropical savanna	Rangpur	2000	279,000	2400.56	Humid sub-tropical	
	2010	786,000				2010	337,000			
	2020	908,000				2020	407,000			
Sylhet	2000	852,000	3452.07	Tropical monsoon						
	2010	529,000								
	2020	331,000								

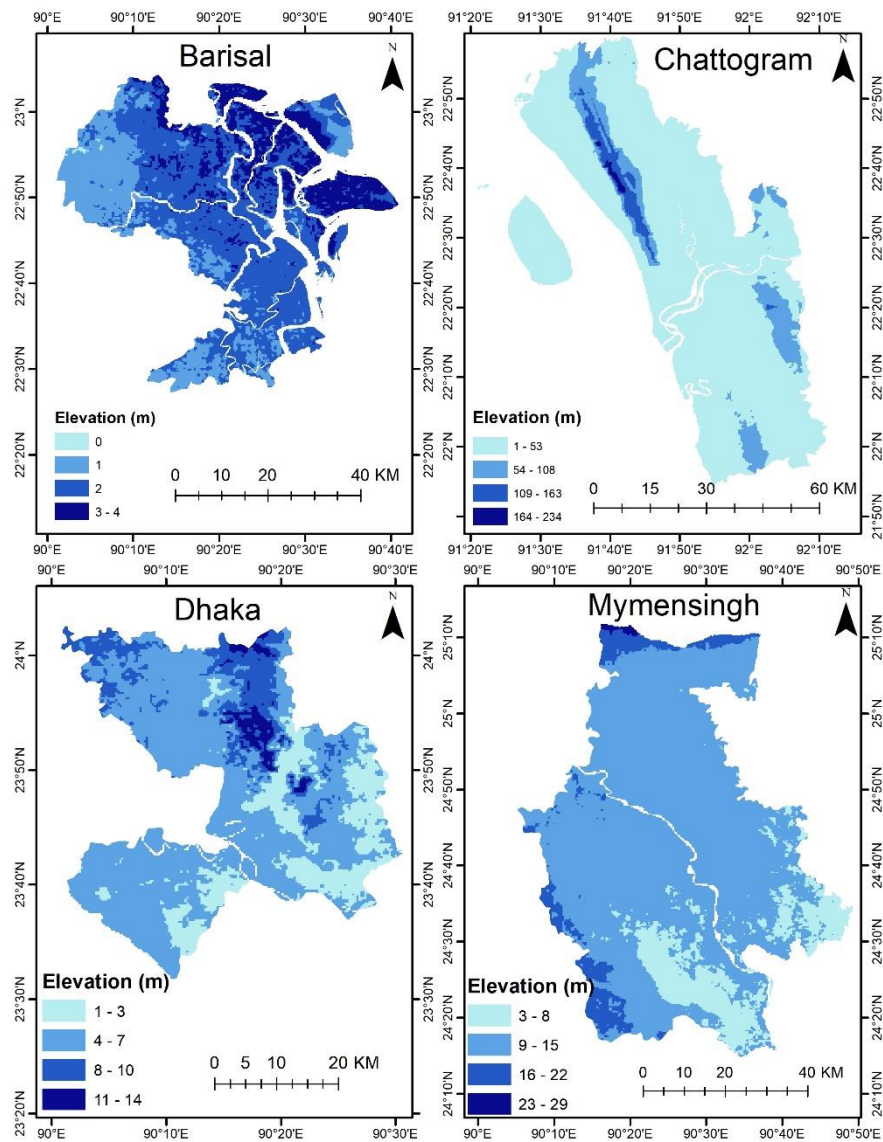


Figure 2. Study area showing four districts, namely Barisal, Chattogram, Dhaka, and Mymensingh, in Bangladesh among seven major districts (digital elevation model).

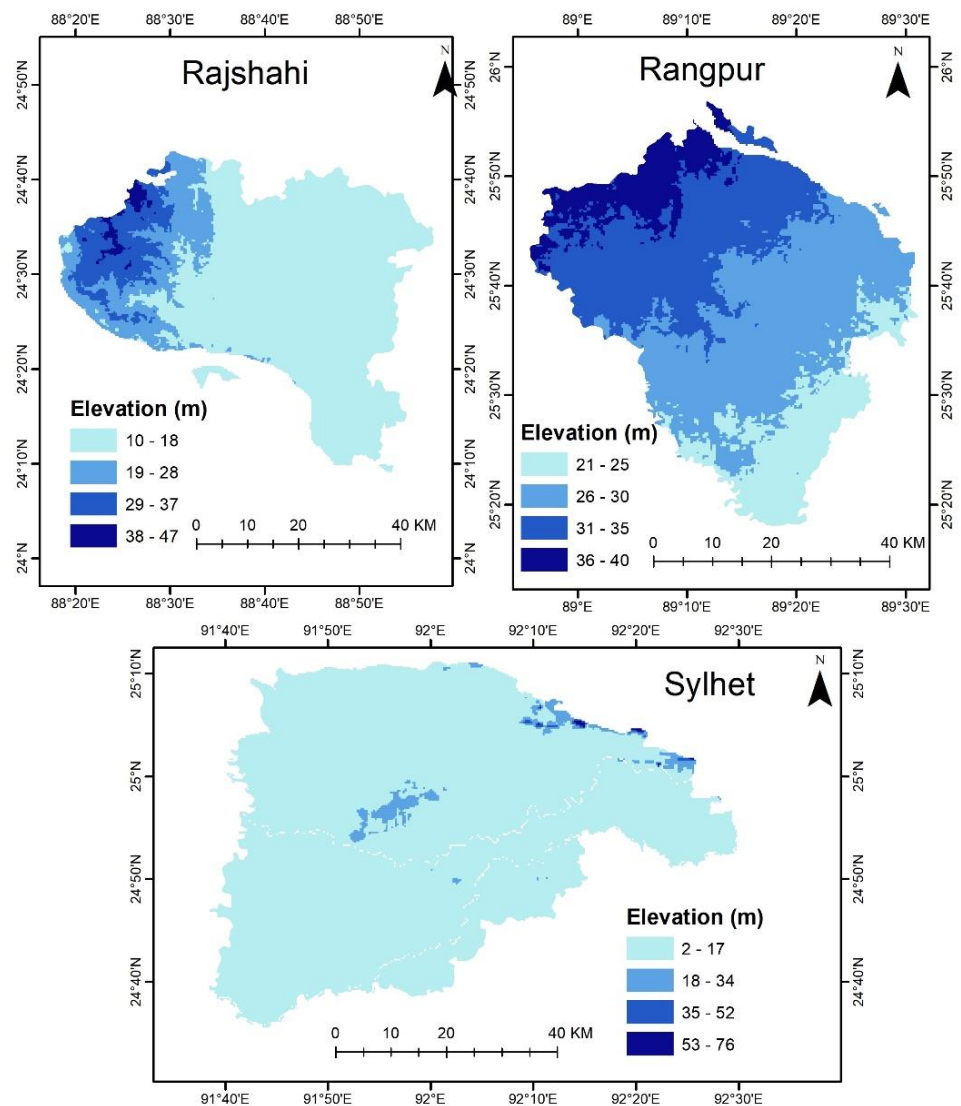


Figure 3. Study area showing remaining three districts including Rajshahi, Rangpur, and Sylhet in Bangladesh, among seven major districts (digital elevation model).

2.2. Data Acquisition and Pre-Processing

For LULC classification, NDVI derivation, LST retrieval, and to detect changes in UHI, Landsat-5 (2000, 2010) and Landsat-8 (2020) imagery data were collected from the United States Geological Survey (USGS) website (<https://earthexplorer.usgs.gov/>; accessed on 20 February 2021) [32,45,46]. This site was also used to collect the digital elevation of the study area. Details regarding the path, row, and the acquisition dates are given in Table 2. All images have a 30 m spatial resolution except band 6 of Landsat-5, which is 120 m, and band 10 and 11 of Landsat-8. To keep a cloud-free environment for this study, every image was collected between 0% to 5% percent cloud level [32,45,46]. ArcMap 10.8 was used for LULC classification, LST and NDVI derivation, and UHI calculation [32,45,46].

2.3. LULC Classification

Landsat-5 and Landsat-8 images were used for LULC classification. The maximum likelihood supervised classification (MLSC) algorithm was used for LULC classification using training sample areas [45]. Bare land, built-up area, vegetation, and water body were the four categories used to classify the images. To generate LULC maps, around 40 to 50 sample areas were collected for each class [46].

Table 2. Landsat image details for this study.

District	Year	Landsat	Date of Acquisition	Sensor	Path and Row
Barisal	2000	Landsat-5	19 January 2000	TM	137/44
	2010		30 January 2010		
	2020		26 January 2010		
Chattogram	2000	Landsat-5	13 February 2000	TM	136/44, 136/45
	2010		8 February 2010		
	2020		4 February 2020		
Dhaka	2000	Landsat-5	19 January 2000	TM	137/43, 137/44
	2010		30 January 2010		
	2020		11 February 2010		
Mymensingh	2000	Landsat-5	19 January 2000	TM	137/43
	2010		30 January 2010		
	2020		11 February 2010		
Rajshahi	2000	Landsat-5	11 February 2000	TM	138/43
	2010		6 February 2010		
	2020		18 February 2020		
Rangpur	2000	Landsat-5	11 February 2000	TM	138/42
	2010		6 February 2010		
	2020		2 February 2020		
Sylhet	2000	Landsat-5	29 February 2000	TM	136/43
	2010		8 February 2010		
	2020		4 February 2020		

2.4. Accuracy Assessment

Accuracy assessment is the procedure used to test the accuracy of computer-classified maps and to view descriptive statistics used to compare classification results with ground information [32]. Around 200–220 points were used as ground observation points to show the validation of the LULC map in the year 2000, 2010, and 2020 in all seven districts [45,47,48]. Those points were validated with Google Earth Pro [45,47,48]. Four classes (bare land, built-up area, vegetation, water body) were identified through computer-classified maps and ground observations. Overall accuracy, user accuracy, producer accuracy, and kappa coefficient were calculated from the error matrix [45,47,48]. The standard kappa coefficient test was carried out to quantify the level of agreement. Accuracy is categorized as good when the kappa coefficient is higher than 0.75 [45]. In this study, the results show that all the accuracy was over 0.75.

2.5. NDVI Derivation

The NDVI method has been extensively used to identify different vegetation types and non-vegetated areas [49]. R (red) and NIR (near-infrared) values are used to calculate it, and it is a ratio of the two [50]. We employed the NDVI to observe the relationship between built-up area and vegetated area changes corresponding with LST.

The NDVI is a measurement of a plant's health based on how it reflects light at specific frequencies (some waves are absorbed, and others are reflected) [13]. Because it compensates for variations in lighting conditions, surface slope, exposure, and other environmental factors, the NDVI is preferred for global vegetation monitoring [13,19,21,22,48]. In this study, we used the NDVI to obtain the vegetation index which is utilized in various studies, whereas the EVI has also proved its advancement [13,19,21,22,48–50]. Therefore,

besides the NDVI, the EVI is preferred for future comparative study in our study area for vegetation indexing.

$$NDVI = (NIR - R)/(NIR + R) \quad (1)$$

where Landsat 4–7, $NDVI = (\text{Band 4} - \text{Band 3})/(\text{Band 4} + \text{Band 3})$. Additionally, Landsat-8, $NDVI = (\text{Band 5} - \text{Band 4})/(\text{Band 5} + \text{Band 4})$.

2.6. LST Derivation for Landsat-5

Thermal band 6 was used for LST calculation for Landsat-5 satellite images in some steps [51]. This can be carried out in three steps.

Step 1 is the conversion of digital number (DN) to Radiance (L_γ):

$$L_\gamma = \left(\frac{LMAX_\gamma - LMIN_\gamma}{QCALMAX - QCALMIN} \right) \times (QCAL - QCALMIN) + LMIN_\gamma \quad (2)$$

where L_γ is spectral radiance, $QCAL$ is the quantized calibrated value in DN, $LMAX_\gamma$ is spectral radiance scaled to $QCALMAX$ in ($W/(m^2 \times sr \times \mu m)$), $LMIN_\gamma$ is spectral radiance scaled to $QCALMIN$ in ($W/(m^2 \times sr \times \mu m)$), $QCALMAX$ is the maximum quantized calibrated pixel value (corresponding to $LMAX_\gamma$) in DN, and $QCALMIN$ is the minimum quantized calibrated pixel value (corresponding to $LMIN_\gamma$) in DN.

Step 2 is the calculation of temperature brightness in kelvin:

$$T_k = \frac{K2}{\ln\left(\frac{K1}{L_\gamma} + 1\right)} \quad (3)$$

where T is the effective at-satellite temperature in kelvin, $K2$ is calibration constant 2, which is 1260.56 for Landsat-5, $K1$ is calibration constant 1, which is 607.76 for Landsat-5, and L_γ is spectral radiance.

Step 3 is the conversion of the temperature to degrees Celsius.

$$T_c = T_k - 273.15 \quad (4)$$

2.7. LST Derivation for Landsat-8

Thermal band 10 was used to collect the land surface temperature for Landsat-8 [52], which can be performed in six steps.

Step 1 is the calculation of the radiance from band 10 [52].

$$L_\gamma = M_L \times QCAL + A_L \quad (5)$$

where L_γ is spectral radiance, M_L is the band-specific multiplicative rescaling factor from the metadata, and A_L is the band-specific additive rescaling factor from the metadata.

Step 2 comes after converting the spectral radiance, which then needs to be converted to atmospheric temperature brightness [53].

$$TB = \frac{K2}{\ln\left(\frac{K1}{L_\gamma} + 1\right)} - 273.15 \quad (6)$$

where TB is the top of the atmospheric brightness temperature in kelvin and $K2$, and $K1$ is the band-specific thermal conversion constant of 1321.0789 and 774.8853.

Step 3 is to calculate $NDVI$, which is essential for calculating LST for Landsat-8. [54]

$$NDVI = \frac{NIR - RED}{NIR + RED} \quad (7)$$

where NIR is band 5 and RED is band 4.

Step 4 is the calculation of the proportion of vegetation using maximum and minimum *NDVI*,

$$P_v = \left(\frac{NDVI - NDVI_{min}}{NDVI_{max} - NDVI_{min}} \right)^2 \quad (8)$$

Step 5 is the calculation of land surface emissivity using *P_v* [55]

$$LSE = 0.004 \times P_v + 0.986 \quad (9)$$

Step 6 is the calculation of land surface temperature in degrees Celsius,

$$T = TB / \left[1 + \left(\gamma \times \frac{TB}{c2} \right) \ln(LSE) \right] \quad (10)$$

where γ is the wavelength of emitted radiance, $c2$ is $h \times c/s = 1.4388 \times 10^{-2} \text{ mK} = 14,388 \text{ } \mu\text{mK}$, where h is Plank's constant, which is $6.626 \times 10^{-34} \text{ Js}$, s is Boltzmann constant, which is $1.38 \times 10^{-23} \text{ J/K}$ and c is the velocity of light which is $2.994 \times 10^3 \text{ m/s}$.

2.8. Estimation of UHI

UHI is often described as the difference between rural and urban areas [56]. This can also be defined by quantification to consider urban surfaces' local and regional climate change [56]. As for calculating the UHI, land surface temperature value was used [45].

$$UHI = \frac{T - T_m}{T_{sd}} \quad (11)$$

where T is LST and T_m is LST mean, and T_{sd} is the standard deviation of LST.

3. Results and Discussion

3.1. LULC and NDVI Variations and Accuracy ASSESSMENT

Spatiotemporal LULC variations in seven districts were categorized in four definitions for 20 years, including the three assessed years of 2000, 2010, and 2020 (Figure 4). The changing pattern depicts rapid urban expansion in heterogeneous formations for Dhaka, Barisal, Mymensingh, Rangpur, and Chattogram, whereas a systematic change was observed in Rajshahi and Sylhet districts. In addition, Rajshahi city development was observed from east to west, and Sylhet was mostly from the center to the southern part. Table 3 is the measurement of change area variates for different classes of LULC. Dynamic expansion of the built-up area was observed for Barisal, ranging from 10.06% to 32.51%, whereas substantial prolongation of the urban area was experienced by Chattogram, Mymensingh, and Rangpur districts, which changed from 2.76% to 14.98%, 3.24% to 18.36%, and 8.02% to 13.22%, respectively, during 2000–2010 and 2010–2020. A sudden notable increase in urban area was found for the megacity of Dhaka 17.36%, which was observed as negative (−0.98%) for 2000–2010. In contrast, large momentous diminution was fostered by Sylhet, presenting 1.45% of urban land in the 2010–2020 period; meanwhile, it was 12.21% during 2000–2010. Furthermore, Rajshahi and Sylhet were influenced by a decreased urban corridor for both upward and downward patterns compared with other districts, which indicate 5.83% to 3.72% and 1.72% to 0.91% throughout in the same period, as mentioned earlier. However, the significant seesaw is also explored for other classes (Table 3). These results corroborate developed urban areas, scattered extensive population, and the zonation of industrial areas as responsible factors for the swell in built-up areas with particularly diminishing vegetation and water sources. Several existing pieces of works of literature extrapolate similar findings [57–59]. However, another investigation in Bangladesh proves Rangpur, Rajshahi, and Sylhet had excessive city growth of 16%, 12%, and 11%, respectively, which slightly contradicts the present study [60]. Additionally, vegetated areas were observed to decrease significantly over all of the seven districts.

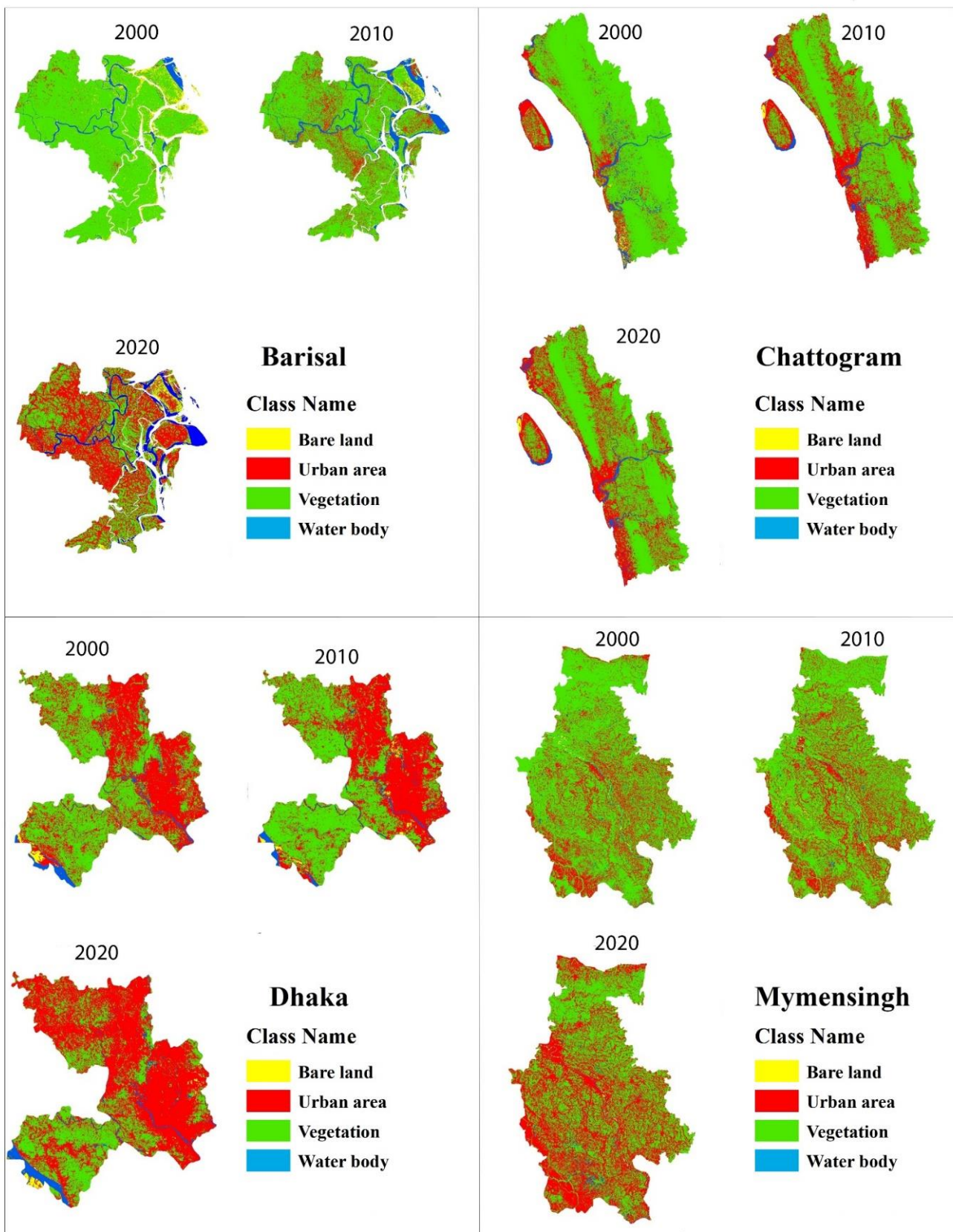


Figure 4. Cont.

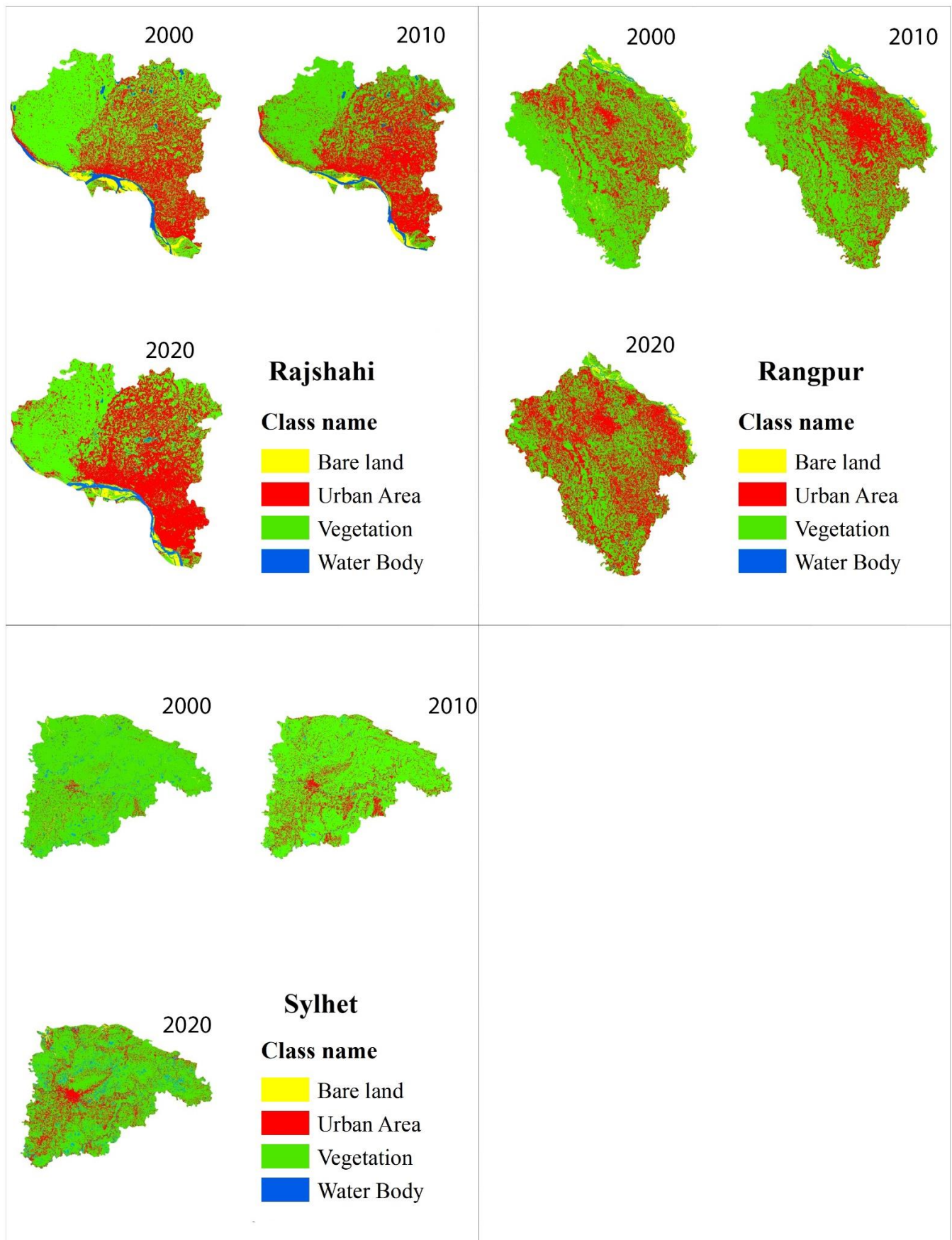


Figure 4. Spatiotemporal distributions of LULC in seven districts of Bangladesh.

Table 3. LULC changed area.

District	Category	2000 (sq.km)	2010 (sq.km)	2020 (sq.km)	Changes (2000–2010)	Percent Changes	Changes (2010–2020)	Percent Changes
Rangpur	Bare Land	58.05	30.69	32.50	−27.36	−1.18	1.81	0.08
	Urban area	573.16	759.75	1067.40	186.59	8.02	307.65	13.22
	Water body	20.11	33.69	29.80	13.58	0.58	−3.89	−0.17
	Vegetation	1675.21	1502.41	1196.78	−172.80	−7.43	−305.63	−13.14
Mymensingh	Bare Land	12.81	44.40	13.37	31.59	0.74	−31.03	−0.72
	Urban area	1094.82	1233.73	2020.48	138.91	3.24	786.75	18.36
	Water body	47.69	47.09	70.23	−0.60	−0.01	23.14	0.54
	Vegetation	3130.21	2960.58	2181.74	−169.63	−3.96	−778.84	−18.17
Sylhet	Bare Land	27.48	2.89	21.33	−24.59	−0.71	18.44	0.53
	Urban area	159.55	580.75	630.70	421.20	12.21	49.95	1.45
	Water body	146.30	65.40	235.87	−80.90	−2.34	170.47	4.94
	Vegetation	3117.64	2801.88	2563.87	−315.76	−9.15	−238.01	−6.90
Rajshahi	Bare Land	54.68	51.76	45.09	−2.92	−0.12	−6.67	−0.28
	Urban area	848.48	987.26	1075.77	138.78	5.83	88.51	3.72
	Water body	75.23	68.04	70.15	−7.19	−0.30	2.11	0.09
	Vegetation	1403.68	1274.90	1191.03	−128.78	−5.41	−83.87	−3.52
Dhaka	Bare Land	14.40	15.89	14.51	1.49	0.10	−1.38	−0.09
	Urban area	709.20	694.21	958.62	−14.99	−0.98	264.41	17.36
	Water body	53.68	48.30	61.63	−5.38	−0.35	13.33	0.88
	Vegetation	745.47	764.40	488.01	18.93	1.24	−276.39	−18.15
Barisal	Bare Land	179.20	63.51	76.70	−115.69	−5.17	13.19	0.59
	Urban area	58.56	295.57	1022.56	237.01	10.60	726.99	32.51
	Water body	107.13	223.79	231.26	116.66	5.22	7.47	0.33
	Vegetation	1891.42	1653.73	905.56	−237.69	−10.63	−748.17	−33.46
Chattogram	Bare Land	40.02	36.63	21.62	−3.39	−0.08	−15.01	−0.33
	Urban area	577.25	701.03	1373.04	123.78	2.76	672.01	14.98
	Water body	184.03	163.30	136.15	−20.73	−0.46	−27.15	−0.61
	Vegetation	3684.43	3584.30	2954.84	−100.13	−2.23	−629.46	−14.03

Figure 5 shows the NDVI variations for the districts considered for the evaluation of the correlations between urban expansion and NDVI reduction during 2000–2020. We found a significant relationship between built-up area and NDVI, which demonstrates areas of the NDVI decreased excessively for Barisal, Dhaka, Mymensingh, Chattogram, and Rangpur, whereas the built-up area increased substantially in the respective areas (Figure 5 and Table 3). In contrast, Rajshahi and Sylhet experienced less NDVI degradation, supported in Table 3, because the urban area was not heavily expanded, resulting in less vegetation loss. Overall, there is a strong and positive correlation between NDVI-estimated areas and the LULC classification assessment.

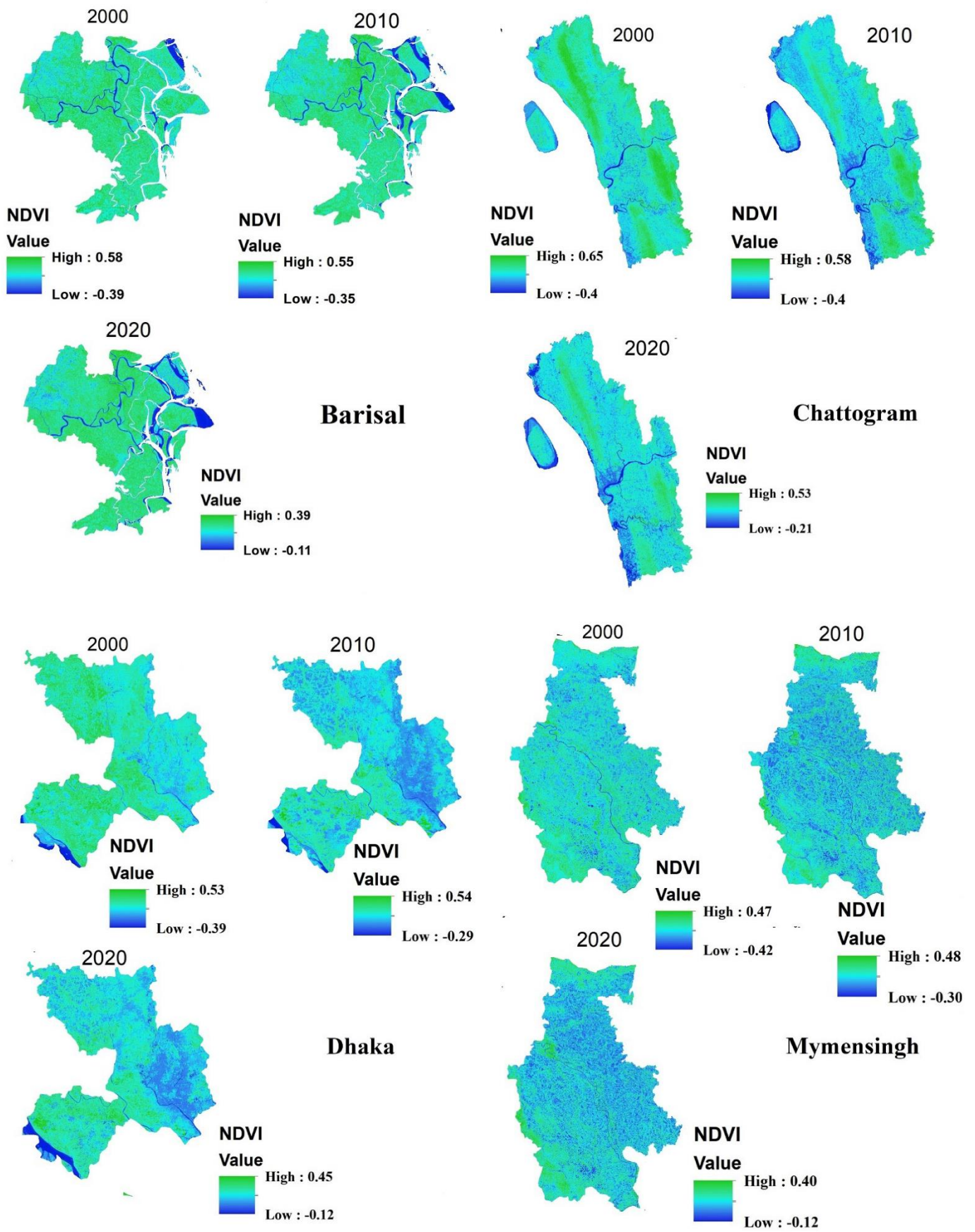


Figure 5. Cont.

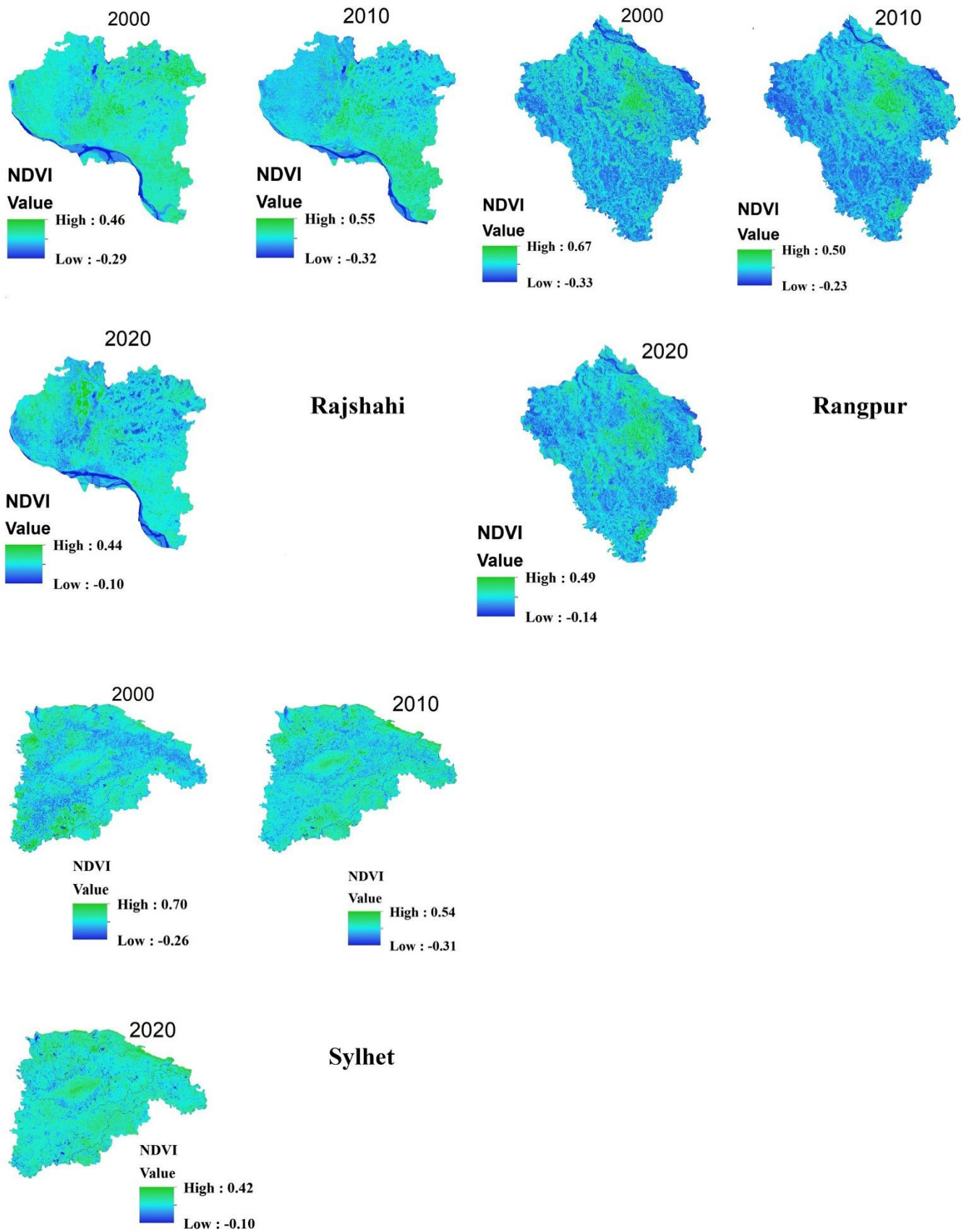


Figure 5. Spatiotemporal distributions of NDVI in seven districts of Bangladesh.

Accuracy evaluation is vital for urban development and the surface's temperature [61]. Congalton used it to determine classification validation. Moreover, accuracy assessment was utilized for the present exploration to validate LULC classification (Table 4). Overall, 200–220 reference points were taken for each district and visualized with the Google Earth Pro engine. The kappa coefficient and overall accuracy values mostly exhibit more than 80 for LULC classes. This estimated value suggests a strong validation demonstration for the study area categorization. Additionally, the kappa coefficient > 0.75 strengthens the very good position of classified accuracy, whereas $40 <$ is defined as poor accuracy [32,61].

Table 4. Accuracy assessment details.

District	Year	Class	User Accuracy	Producer Accuracy	Overall Accuracy	Kappa Coefficient
Barisal	2000	Bare Land	73.68	82.35	85.20	0.77
		Built-up Area	66.67	90.91		
		Vegetation	94.05	79.83		
		Water Body	94.29	100.00		
	2010	Bare Land	88.57	100.00	88.00	0.81
		Built-up Area	73.68	70.00		
		Vegetation	76.60	90.00		
		Water Body	95.96	87.16		
	2020	Bare Land	87.50	100.00	93.13	0.90
		Built-up Area	97.50	90.70		
		Vegetation	87.50	87.50		
		Water Body	100.00	95.24		
Chattogram	2000	Bare Land	77.50	91.18	81.88	0.75
		Built-up Area	85.00	75.56		
		Vegetation	85.00	69.39		
		Water Body	80.00	100.00		
	2010	Bare Land	80.00	80.00	83.13	0.77
		Built-up Area	80.00	80.00		
		Vegetation	87.50	87.50		
		Water Body	85.00	85.00		
	2020	Bare Land	92.50	94.87	86.88	0.82
		Built-up Area	75.00	75.00		
		Vegetation	87.50	81.40		
		Water Body	92.50	97.37		
Dhaka	2000	Bare Land	82.50	100.00	83.75	0.78
		Built-up Area	85.00	77.27		
		Vegetation	80.00	71.11		
		Water Body	87.50	92.11		
	2010	Bare Land	90.00	100.00	91.25	0.88
		Built-up Area	92.50	78.72		
		Vegetation	85.00	89.47		
		Water Body	97.50	100.00		
	2020	Bare Land	90.00	100.00	86.88	0.82
		Built-up Area	80.00	76.19		
		Vegetation	80.00	78.05		
		Water Body	97.50	95.12		

Table 4. Cont.

District	Year	Class	User Accuracy	Producer Accuracy	Overall Accuracy	Kappa Coefficient
Mymensingh	2000	Bare Land	85.00	100.00	88.13	0.84
		Built-up Area	92.50	92.50		
		Vegetation	85.00	72.34		
		Water Body	90.00	92.31		
	2010	Bare Land	82.50	97.06	83.13	0.77
		Built-up Area	67.50	100.00		
		Vegetation	87.50	92.11		
		Water Body	95.00	62.30		
	2020	Bare Land	87.50	100.00	88.75	0.85
		Built-up Area	97.50	88.64		
		Vegetation	87.50	79.55		
		Water Body	82.50	89.19		
Rajshahi	2000	Bare Land	100.00	95.24	87.50	0.83
		Built-up Area	80.00	94.12		
		Vegetation	80.00	74.42		
		Water Body	90.00	87.80		
	2010	Bare Land	100.00	95.24	89.38	0.85
		Built-up Area	67.50	96.43		
		Vegetation	97.50	73.58		
		Water Body	92.50	100.00		
	2020	Bare Land	100.00	100.00	93.13	0.90
		Built-up Area	82.50	94.29		
		Vegetation	92.50	82.22		
		Water Body	97.50	97.50		
Rangpur	2000	Bare Land	80.00	100.00	87.50	0.83
		Built-up Area	82.50	80.49		
		Vegetation	90.00	76.60		
		Water Body	97.50	97.50		
	2010	Bare Land	95.00	100.00	90.00	0.86
		Built-up Area	85.00	91.89		
		Vegetation	90.00	76.60		
		Water Body	90.00	94.74		
	2020	Bare Land	90.00	94.74	86.88	0.82
		Built-up Area	77.50	83.78		
		Vegetation	82.50	71.74		
		Water Body	97.50	100.00		

Table 4. Cont.

District	Year	Class	User Accuracy	Producer Accuracy	Overall Accuracy	Kappa Coefficient
Sylhet	2000	Bare Land	72.50	100.00	87.50	0.83
		Built-up Area	87.50	85.37		
		Vegetation	95.00	80.85		
		Water Body	95.00	88.37		
	2010	Bare Land	100.00	97.56	91.25	0.88
		Built-up Area	97.50	75.00		
		Vegetation	72.50	100.00		
		Water Body	95.00	100.00		
	2020	Bare Land	82.50	97.06	84.38	0.79
		Built-up Area	82.50	82.50		
		Vegetation	95.00	71.70		
		Water Body	77.50	93.94		

3.2. Assessment of LST

Figure 6 and Table 5 demonstrate the spatiotemporal change measurement of land surface temperature in the study period of 2000, 2010, and 2020. Extreme land surface temperature due to compact developed areas depicts the hotspots zones of the respective location. LULC mutation and LST transformation are equivalent in temporal and spatial depiction between the stated period. Barisal district had a large area of temperature change ranging from 17 to 18 °C (>45% area) in 2000, wherein in two decades, it increased to 18–20 °C (>68% area). This corresponds to Figures 4–6 and Table 5, which signifies expanded urbanized and dryland areas causing an increase in temperature; hence, hotspot areas (Figure 7) were primarily found in those two LULC categorized areas. Similarly, in the Chattogram district, dominating scatter LST formation found which depicted >32% area of 20–21 °C in 2000 as it increased in 2020, with a >55% area enlargement of 21–23 °C, which compares identical built-up and bare land area extension (Figure 4 and Table 3). In 2000, Dhaka's more significant portion (43% area) was 16–17 °C; a rapid increase was observed in 2010 that sustained until 2020, comprising 20–23 °C for the prolonged area of 66%. Additionally, Mymensingh represented a high concentrated temperature zone along the riverside in bare land and the developed area (Figures 4 and 6), validated by Figure 7 of the hotspot zones of the respective area. A gradual upward trend of temperature augmentation was also observed for Mymensingh from 2000 to 2020 in the range of 17–18 °C (>60% area) to 20–22 °C (>70% area). Furthermore, for the Sylhet district, the LST threshold remained 16–24 °C, which was significant in the proximate sense for the entire echelon of exploration (Figure 5 and Table 5). Due to acknowledged heterogenous urban and bare land (Figure 4), hotspots of the Sylhet district remained interspersed in 4.42% of the area in 2020 (Table 5). Ordinary change of LST precipitated for Rangpur district that sustained 18–20 °C for the utmost territory during the same study period with a deficient hotspot area of 4.47% (Figures 6 and 7 and Table 5).

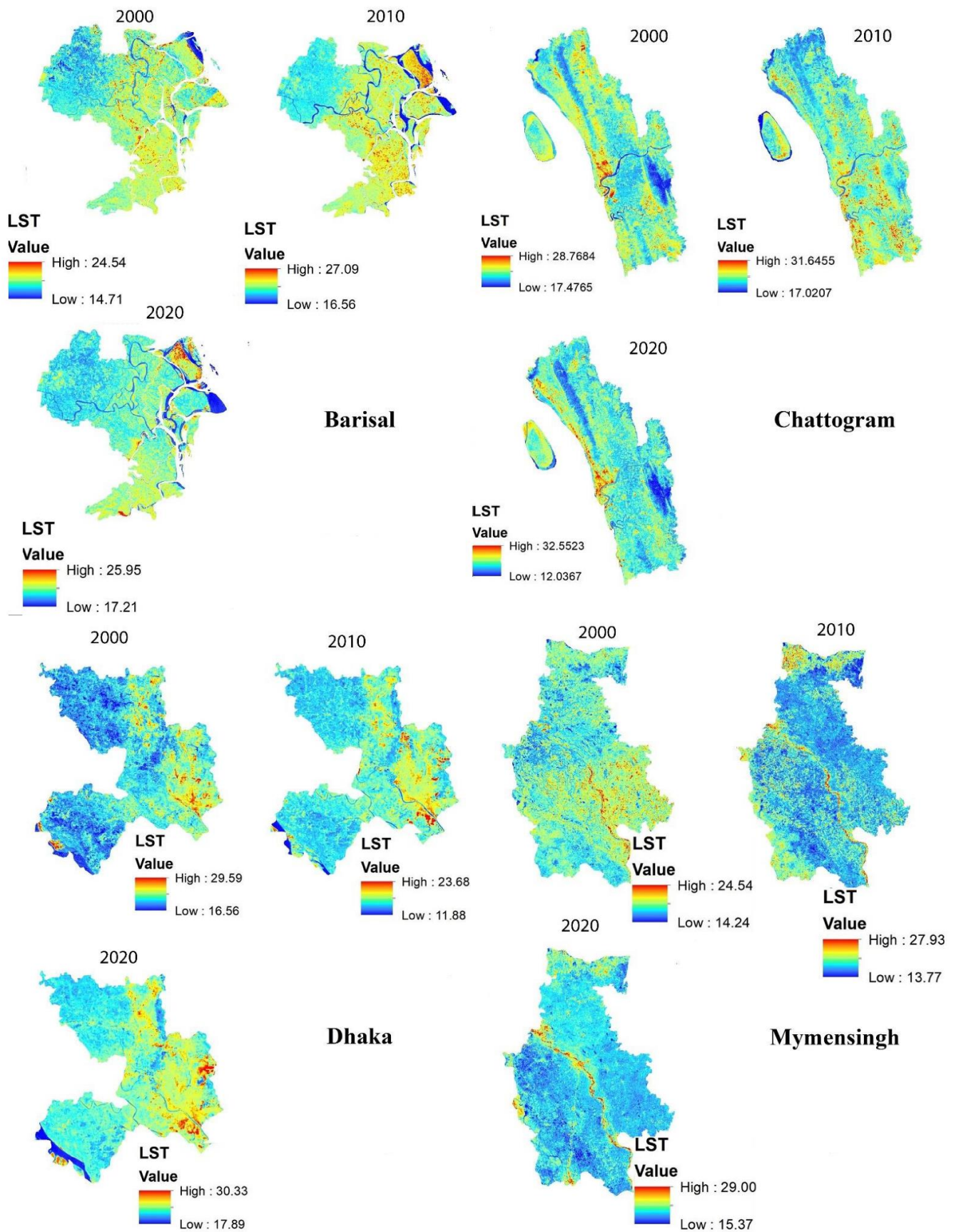


Figure 6. Cont.

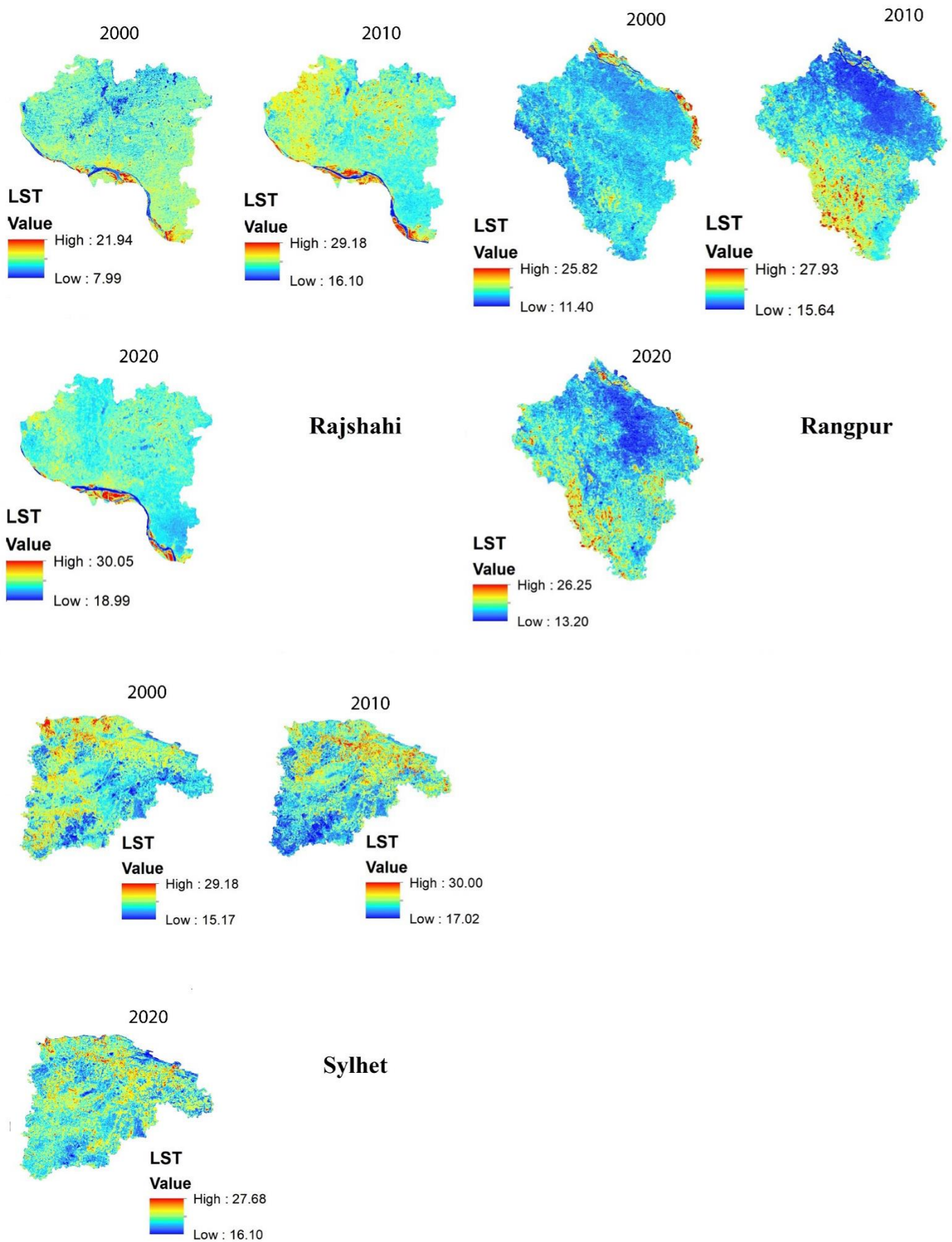


Figure 6. Spatiotemporal distributions of LST in seven districts of Bangladesh during 2000–2020.

Table 5. LST area distribution.

Area	Year	Temperature (°C)	Area	Per Cent Change	Area	Year	Temperature (°C)	Area	Per Cent Change		
Barisal	2000	14.71–17.47	312.96	13.99	Chattogram	2000	17.47–20.17	799.2422	17.82		
		17.47–18.38	1007.304	45.04			20.17–21.06	1477.061	32.93		
		18.38–18.83	544.7676	24.36			21.06–21.94	1332.5	29.71		
		18.83–19.72	325.35	14.55			21.94–23.25	780.1382	17.39		
		19.72–24.54	46.23	2.07			23.25–28.76	96.631	2.15		
	2010	16.56–17.93	149.85	6.70		2010	17.02–21.06	799.2604	17.82		
		17.93–19.72	700.18	31.31			21.06–22.37	1607.954	35.85		
		19.72–21.06	960.27	42.93			22.37–23.68	1232.395	27.47		
		21.06–22.37	362.99	16.23			23.68–25.82	706.7859	15.76		
		22.37–27.09	63.28	2.83			25.82–31.64	139.27	3.10		
		2020	17.21–18.61	207.8975			9.30	2020	12.03–20.05	569.3204	12.69
			18.61–19.39	763.3504			34.13		20.05–21.01	1477.769	32.94
19.39–20.08	766.6907		34.28	21.01–21.97	1383.896	30.85					
20.08–21.13	445.1029		19.90	21.97–23.33	840.1881	18.73					
21.13–25.95	53.52764		2.39	23.33–32.55	213.0636	4.75					
Dhaka	2000	11.88–16.10	169.3025	11.12	Mymensingh	2000	14.24–17.02	935.6212	21.83		
		16.10–17.02	660.2207	43.35			17.02–17.93	1672.55	39.03		
		17.02–17.93	444.6282	29.20			17.93–18.83	1204.605	28.11		
		17.93–18.83	181.3708	11.91			18.83–19.72	360.5033	8.41		
		18.83–23.68	67.30422	4.42			19.72–24.54	112.4708	2.62		
	2010	16.53–19.72	398.6277	26.18		2010	13.77–19.28	1117.137	26.07		
		19.72–21.06	623.056	40.91			19.28–20.17	1739.536	40.59		
		21.06–22.37	334.1014	21.94			20.17–21.06	782.3379	18.25		
		22.37–24.11	130.523	8.57			21.06–22.37	508.4115	11.86		
		24.11–29.59	36.50096	2.40			22.37–27.93	138.2994	3.23		
		2020	17.89–20.82	167.0037			10.97	2020	15.37–20.70	657.0212	15.33
			20.82–22.09	592.2974			38.89		20.70–21.28	1911.871	44.61
22.09–23.31	437.5772		28.73	21.28–22.13	1284.027	29.96					
23.31–25.11	258.5014		16.98	22.13–23.68	369.288	8.62					
25.11–30.33	67.40691		4.43	23.68–29.00	63.56586	1.48					
Rajshahi	2000	7.99–13.77	0.108031	0.00	Rangpur	2000	11.40–18.38	532.9292	22.91		
		13.77–16.56	177.5506	7.45			18.38–18.83	761.79	32.74		
		16.56–17.02	507.7203	21.31			18.83–19.72	839.1335	36.07		
		17.02–17.47	1139.577	47.84			19.72–21.06	147.5184	6.34		
		17.47–21.94	557.0388	23.38			21.06–25.82	45.1306	1.94		
	2010	16.10–18.38	47.39137	1.99		2010	15.64–17.93	489.0469	21.02		
		18.38–20.61	932.7005	39.16			17.93–19.28	862.8425	37.09		
		20.61–21.94	776.454	32.60			19.28–20.61	597.2121	25.67		
		21.94–24.11	497.7213	20.89			20.61–22.37	304.2014	13.08		
		24.11–29.18	127.7852	5.36			22.37–27.93	73.21678	3.15		
		2020	18.99–21.28	52.85249			2.22	2020	13.20–18.50	502.6909	21.61
			21.28–22.79	865.2631			36.32		18.50–19.37	821.9776	35.33
22.79–23.83	1077.733		45.24	19.37–20.29	594.9595	25.57					
23.83–25.86	327.451		13.75	20.29–21.51	302.883	13.02					
25.86–30.05	58.75703		2.47	21.51–26.25	103.9618	4.47					

Table 5. Cont.

Area	Year	Temperature (°C)	Area	Per Cent Change	Area	Year	Temperature (°C)	Area	Per Cent Change
Sylhet	2000	15.17–18.83	648.0724	18.78					
		18.83–20.17	988.2278	28.64					
		20.17–21.50	987.1232	28.60					
		21.50–23.25	691.1813	20.03					
		23.25–29.18	136.3068	3.95					
	2010	17.02–20.17	901.1923	26.11					
		20.17–21.50	920.6859	26.68					
		21.50–22.81	824.0293	23.88					
		22.81–24.54	602.0792	17.45					
		24.54–30.00	202.9232	5.88					
	2020	16.10–19.17	607.4081	17.60					
		19.17–19.99	1113.531	32.27					
		19.99–20.80	918.7201	26.62					
		20.80–21.80	658.5974	19.08					
		21.80–27.68	152.66	4.42					

In contrast to the other six districts of Bangladesh, Rajshahi, which experienced less urban expansion (Table 3), showed LST hotspots of 2.47% area, while gradual temperature improvement was noticed from 2000 to 2020, whereas 2010 was found to be stretched for LST, as well as the highly concentrated urban area (Figures 6 and 7 and Table 5). These results conclude that Dhaka and Chattogram are highly concentrated urban areas with intense land surface temperature; hence, they retain greater hotspot zones. Similarly, diversified surface temperatures are acknowledged for different cities in Bangladesh including Chattogram [62,63], Dhaka [58], Rajshahi [45,64,65], Barisal [66], and Mymensingh [67]. The obtained identification determines that dry land considers high LST values as well as urbanized areas, which is shown in the exploration of several studies [45,63]. As each district advances, urban expansion in Bangladesh is the key reason for rainwater infiltration and potential water flow, leading to groundwater deficiency. Moreover, these multipliers cause abnormal water cycles due to evaporation–transpiration disharmonious phenomenon.

Consequently, the water cycle degrades, resulting in environmental change [68]. Thus, it affects the study area's maximum and minimum temperature fluctuations [22]. Aerosol pollution and landscape albedo variations are accompanied by excessive land usage. As a result, land-use reform is one of the worst fundamental cognitive biases that could compromise the planet's radioactive equilibrium [69]. For instance, warm air levels decrease significantly during the transformation of swamp surfaces to cropland, corresponding to extreme albedo rates [70].

Urban expansion influences the minimum temperature to a greater extent than the maximum temperature in the winter season, and this decrease in temperature variations in the winter period has been earlier reported by several researchers [71,72]. In [73], Huang stated that the intensity of LST is elevated because of rapid urbanization in China, causing a higher daily temperature variation in Beijing compared to Shanghai. So, LULC change is the main disquiet; the major districts of Bangladesh have likely faced a higher degree of variation than other areas worldwide, a rate mainly driven by elevated rural–urban migration strategies [74].

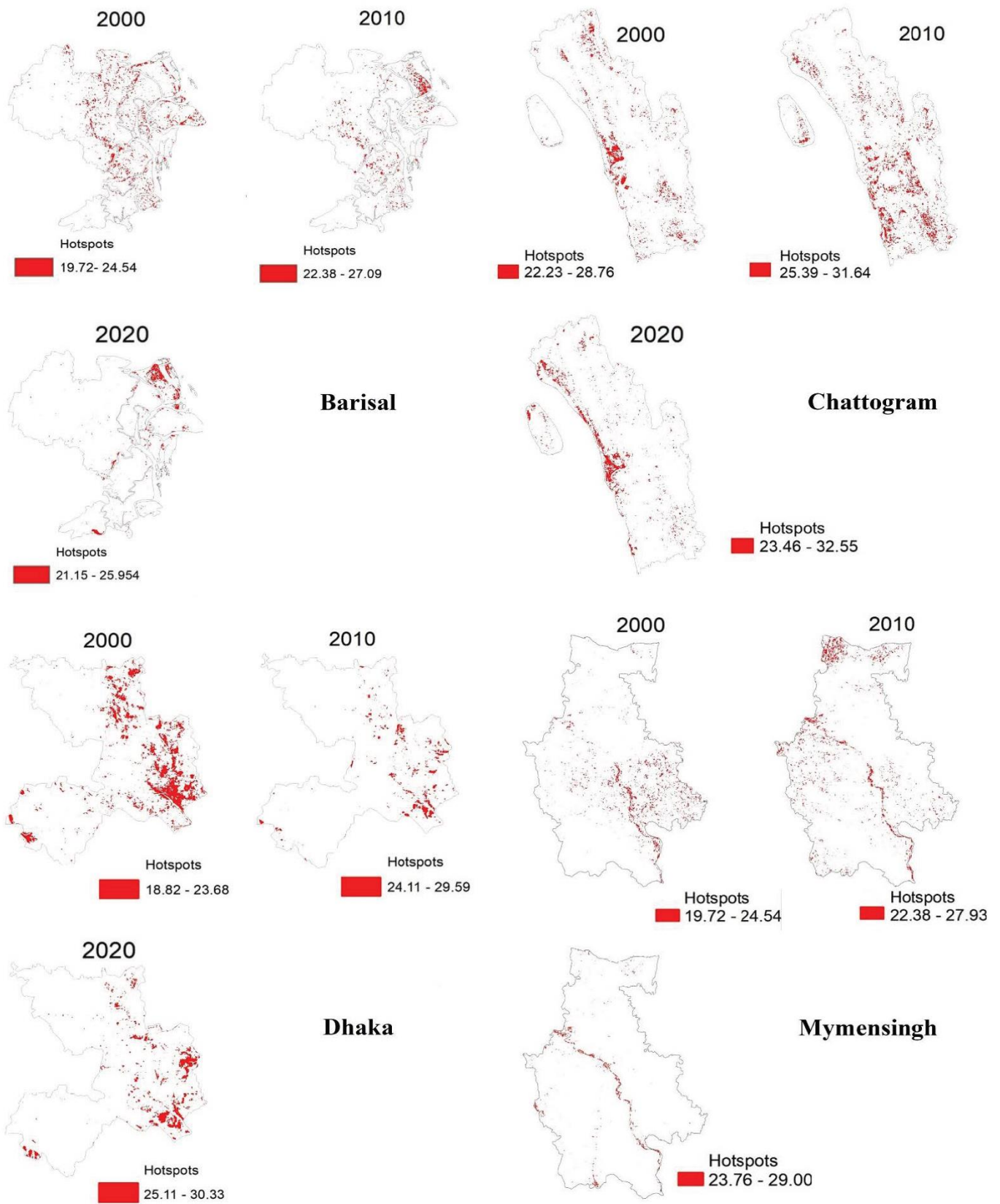


Figure 7. Cont.

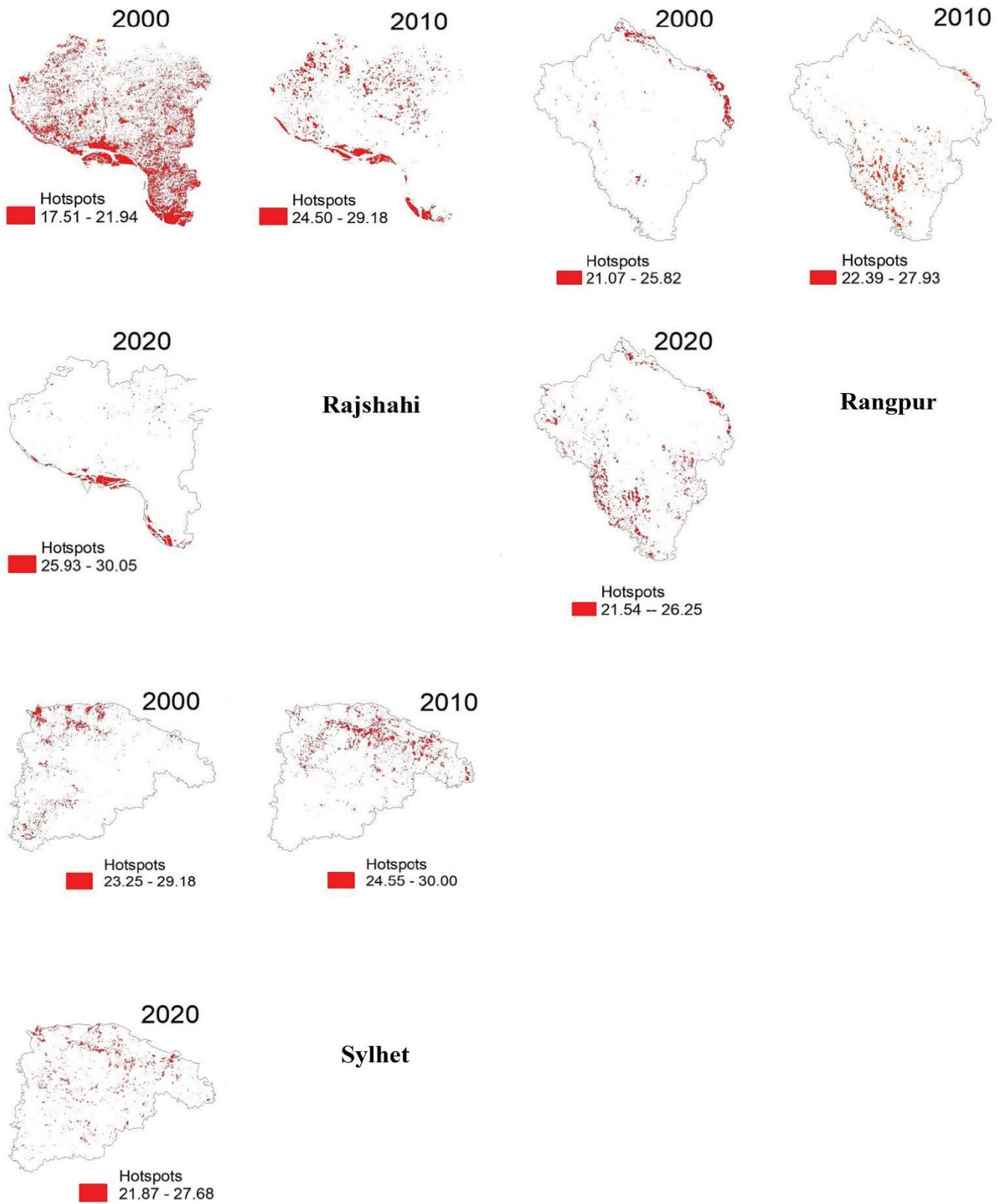


Figure 7. Identified hotspots for seven major districts of Bangladesh during 2000–2020.

3.3. UHI Intensity Assessment

The UHI intensity graph for the seven significant districts of Bangladesh depicts diversified intensity for each location (Figures 8 and 9). The topmost increase in intensity is observed for Mymensingh, 2.81 °C to 10.8 °C, from 2000 to 2020. Moreover, substantial amplification was noticed for Chattogram and Sylhet, observed as 9.65 °C and 7.74 °C. Consequently, in 2020, Barisal retained approximately the same 8.220 C intensity as in 2000, whereas Dhaka indicated a reduction of 1.46 °C as it was 6.95 °C in 2000.

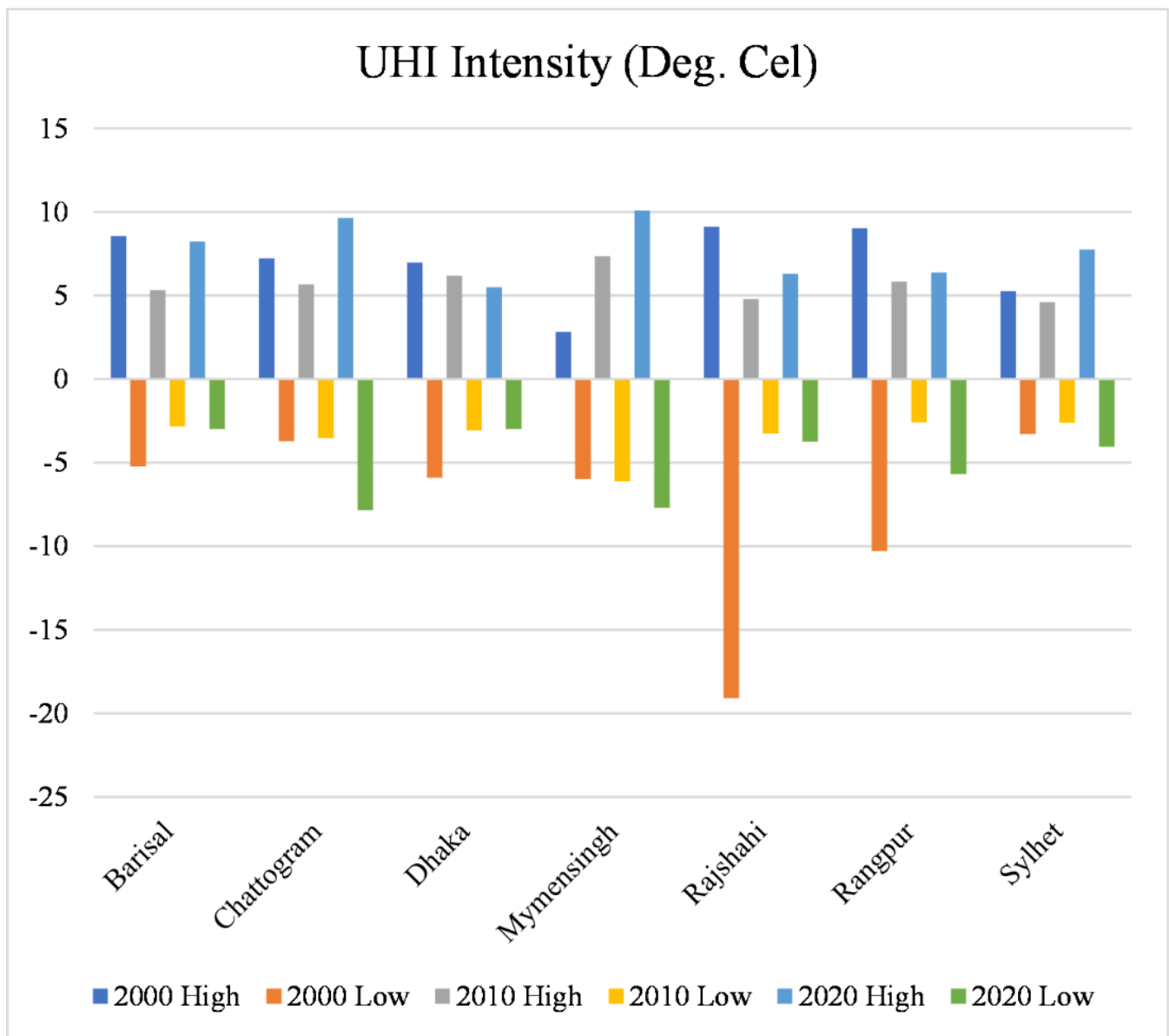


Figure 8. UHI intensity for seven major districts of Bangladesh during 2000–2020.

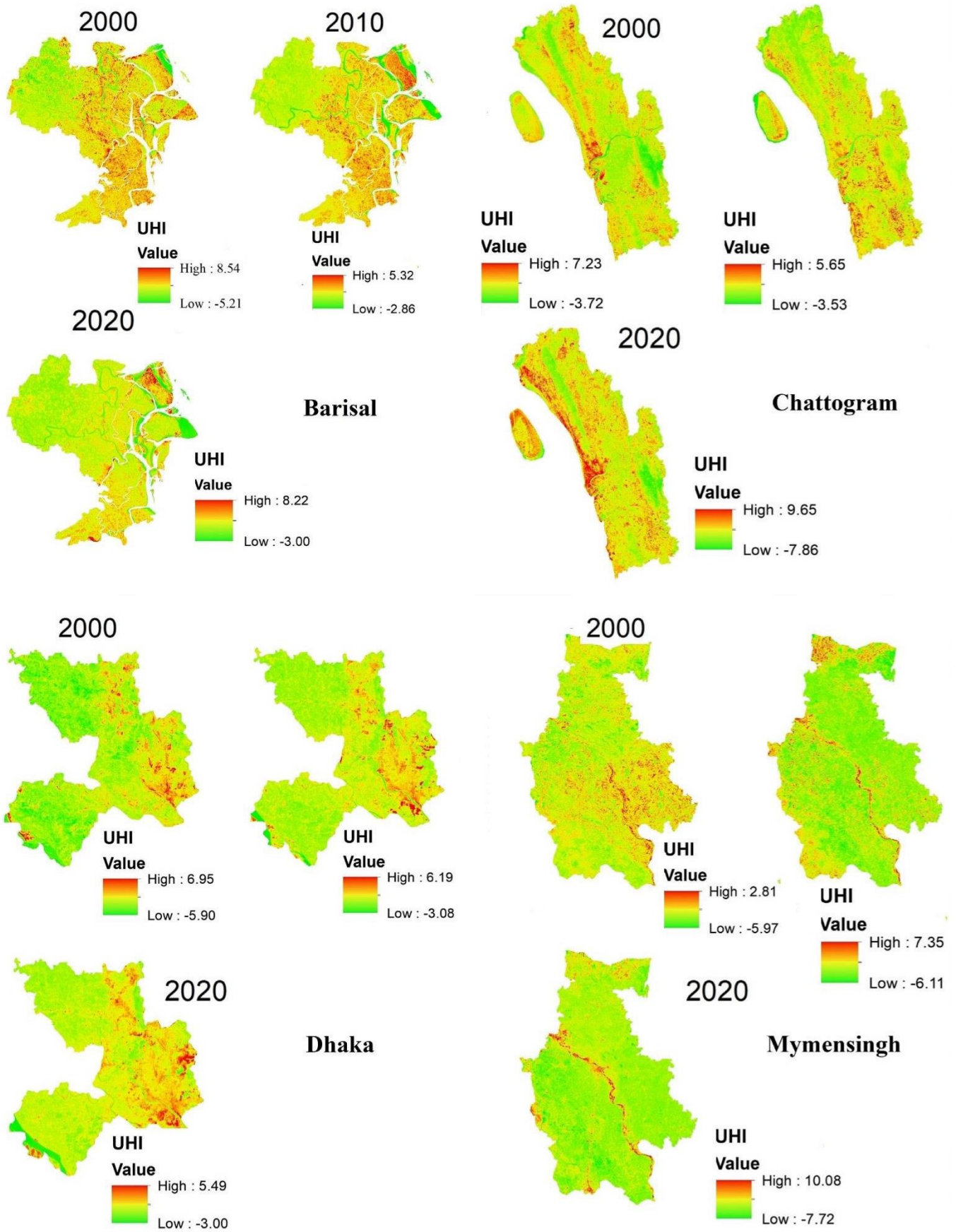


Figure 9. Cont.

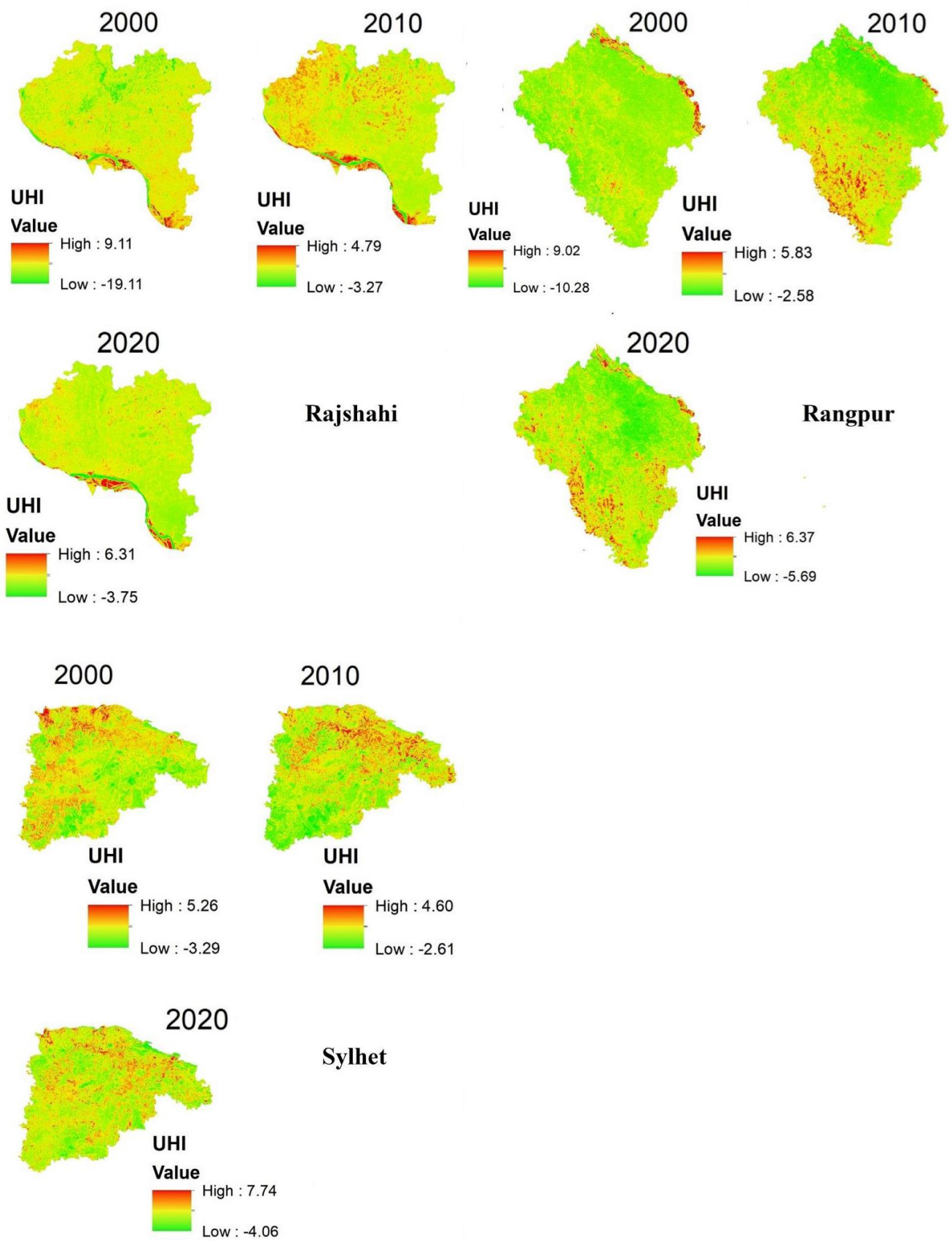


Figure 9. Spatiotemporal distributions of UHI intensity in seven districts of Bangladesh during 2000–2020.

In contrast, Rajshahi and Rangpur alleviated their temperature intensities notably from 9.11 °C to 6.31 °C and 9.02 °C to 6.37 °C, accordingly, from 2000 to 2020. Figure 8 provides an accurate spatiotemporal demonstration of heat intensity regarding the particular study area's industrious, populated, and dry land. The aggregated UHI intensity also corresponds with the illustration of hotspots shown in Figure 7 for each aerial and temporal distribution. [36] Dewan also found the same results as those reported in the present investigation, which determines high intensity in the core of urban areas due to heavy anthropogenic force, population, and fewer vegetated areas of five major cities of Bangladesh: Dhaka, Chattogram, Khulna, Rajshahi, and Sylhet. Thus, the effect of UHI on winter temperature is evident. The temporal changes of UHI could be linked with fast LULC variation and crop phenological change [75], a decline of reference evapotranspiration because of a lot of impervious layers [76], and disparity cooling rates during the winter period [77]. The main difference in delineating the selected urban coverage is a probable area of UHI changes. In [45], an increase of >37% surface temperature caused by the built-up area of Rajshahi was revealed, which validates the UHI observation. Furthermore, a canopy describes dwellings and cycle lanes within a built environment [78]. In general, region-specific UHI works of the country are still lacking except for one study [36]; however, earlier cited works [78] using a chosen Landsat dataset have reported an enhanced UHI, following the present outcomes. Earlier works have focused on the greenness activity in regulating surface temperature, especially during the daytime in the summer [79–82]. The cooling ability of an urban region is commonly regulated by differences in evaporation cooling potential, changes in LULC, the lack of moisture content, and the absence of vegetation cover [83,84].

4. Possible Implication and Limitation of the Study

Fast population growth and the related urban districts are considered pivotal drivers of local and regional temperature variations [85], particularly in developing countries such as Bangladesh. Urbanization coupled with global climate warming will likely enhance heat-associated mortality events [86]. A normal urban district in Bangladesh is characterized by few tree plantations and highly scattered vegetated areas [87]. Tree coverage might be of aid in enhancing cooling activities. The cooling impacts of vegetation rely on vegetation types. For example, green vegetation is noticeably more efficient in giving year-round advantages than other vegetation types [88]. This study gave reference datasets on the seasonal intensity of UHI during the winter dry season, and larger districts seem to have higher variation than smaller districts. The outcomes of our research are anticipated to give vital information for future study, provided that global climate warming is possible to exacerbate UHI impacts in the forthcoming period. This research aids advancement towards the United Nation's SDGs and the regional climate information found in this work can support the generation of district-specific adaptation strategies.

Several drawbacks to this work should not be overlooked. First, the only remote-sensing-derived index was adopted to identify UHI over major districts of Bangladesh. The climatic variables [89], landscape metrics [80], and clear albedo [90] can make further study more effective, as the parameters could have a substantial influence on LST. Second, since UHI has considerable daily and seasonal variations, which would also be of great value, we only considered the winter period and thus limited its wide application. Third, the problem of lessening pixel values due to a lack of clear sky is noticed most remarkably in the winter period in Bangladesh, and thus the effect on LST and derived UHI intensity is most evident in that season. In general, the application of in situ arrangement can also be applied to estimate the validation of LST extents. Ultimately, it is worth mentioning that the outcomes obtained from our research are based on high-resolution satellite imageries assessment using remote sensing tools, and the measured LST is not verified with the actual ground condition. Despite these drawbacks, this research gives a better understanding of the local temperature changes and global warming within the large districts of Bangladesh

and gives further information for developing potential mitigation actions. However, this deserves further investigation.

5. Conclusions

This research aimed to investigate LULC, NDVI, and LST variations concerning UHI intensity diversification over Bangladesh's seven most populated urbanized districts, combining 20 years of quality-controlled LULC and LST datasets. The MLSC algorithm was employed to measure the LULC category with good precision (81–93%). The results indicated that a significant reduction in vegetated land was observed at the expense of built-up areas in all districts except for Rajshahi and Sylhet. In the winter season, LST had increased from 3 °C to 8 °C during the study period. The LST patterns indicate that built-up areas under urban expansion exhibited high LST, while the vegetated area and water bodies depicted relatively low LST. Our study revealed that the UHI intensities appeared to be increasing, which might mean the narrowing of the diurnal temperature range. The UHI intensities for all districts were found to vary from 8 °C to 10 °C. Analysis showed that the magnitude of UHI intensity was high for Mymensingh (10 °C) and low for Dhaka (1.46 °C). These changes will substantially affect the regional climate change of these districts, which highlights significant thermal variations present in all district areas. This study identified significant hotspots zones and UHI intensity in densely populated urban dwellings and low moisture content area/dry, bare land. The outcome of our research is anticipated to give crucial information for future work, provided that global warming is expected to exacerbate UHI impacts in the forthcoming period. A practical initiative to a city decentralization policy is suggested. Governments, the NGO sector, climate scientists, urban planners, and engineers could consider the potential findings of this study for sustainable climate and urban design purposes. Our study confirms development towards the UN's SDGs (sustainable development goals), and the local climate information in our study could aid in developing district-specific mitigation strategies.

Author Contributions: Conceptualization, M.N.R.; methodology, M.N.R. and F.A.J., and M.R.H.R.; software, M.N.R.; validation, S.C.P., M.S.I., E.A. and M.N.R.; formal analysis, M.N.R. and M.R.H.R.; investigation, M.N.R.; resources, M.N.R.; data curation, M.N.R.; writing—original draft preparation, M.N.R. and A.R.M.T.I.; writing—review and editing, S.C.P. and M.N.R.; visualization, M.N.R. and F.A.J.; supervision, A.R.M.T.I. and M.N.R.; project administration, M.N.R.; funding acquisition, E.A. All authors have read and agreed to the published version of the manuscript.

Funding: The authors gratefully acknowledge the generous philanthropic support from the Office of the Vice President of the Rabdan Academy, the United Arab Emirates (UAE).

Institutional Review Board Statement: Not applicable.

Informed Consent Statement: Not applicable.

Data Availability Statement: Not applicable.

Acknowledgments: The authors would like to thank the US Geological Survey (USGS) for assisting this research with datasets.

Conflicts of Interest: There is no conflict of interest to publish this work.

References

1. Muñoz, P.; Zwicky, S.; Mirzabaev, A. The impact of urbanization on Austria's carbon footprint. *J. Clean. Prod.* **2020**, *263*, 121326. [[CrossRef](#)]
2. Seto, K.C.; Dhakal, S.; Bigio, A.; Blanco, H.; Delgado, G.C.; Dewar, D.; Huang, L.; Inaba, A.; Kansal, A.; Lwasa, S.; et al. Human settlements, infrastructure, and spatial planning. In *Climate Change 2014: Mitigation of Climate Change. IPCC Working Group III Contribution to AR5*; Cambridge University Press: Cambridge, MA, USA, 2014.
3. United Nations. *68% of the World Population Projected to Live in Urban Areas by 2050*; UN: New York, NY, USA, 2018.
4. Chapman, S.; Thatcher, M.; Salazar, A.; Watson, J.; McAlpine, C.A. The impact of climate change and urban growth on urban climate and heat stress in a subtropical city. *Int. J. Clim.* **2019**, *39*, 3013–3030. [[CrossRef](#)]

5. Abir, F.A.; Ahmmed, S.; Sarker, S.H.; Fahim, A.U. Thermal and ecological assessment based on land surface temperature and quantifying multivariate controlling factors in Bogura, Bangladesh. *Heliyon* **2021**, *7*, e08012. [[CrossRef](#)]
6. Morshed, S.R.; Fattah, A. Responses of spatiotemporal vegetative land cover to meteorological changes in Bangladesh. *Remote Sens. Appl. Soc. Environ.* **2021**, *24*, 100658. [[CrossRef](#)]
7. Roy, B.; Bari, E.; Nipa, N.J.; Ani, S.A. Comparison of temporal changes in urban settlements and land surface temperature in Rangpur and Gazipur Sadar, Bangladesh after the establishment of city corporation. *Remote Sens. Appl. Soc. Environ.* **2021**, *23*, 100587. [[CrossRef](#)]
8. Egerer, M.H.; Lin, B.B.; Threlfall, C.G.; Kendal, D. Temperature variability influences urban garden plant richness and gardener water use behavior, but not planting decisions. *Sci. Total Environ.* **2018**, *646*, 111–120. [[CrossRef](#)]
9. Ayanlade, A. Remote sensing approaches for land use and land surface temperature assessment: A review of methods. *Int. J. Image Data Fusion* **2017**, *8*, 188–210. [[CrossRef](#)]
10. Rahman, M.Z.; Rashid, M.S. Aerial Extent Analysis and Environmental Problems Identification of Matasagar and Sukhsagar Wetlands in Bangladesh Using GIS and Remote Sensing Tools. *J. Geogr. Inf. Syst.* **2016**, *8*, 683–691. [[CrossRef](#)]
11. Saaroni, H.; Ben-Dor, E.; Bitan, A.; Potchter, O. Spatial distribution and microscale characteristics of the urban heat island in Tel-Aviv, Israel. *Landsc. Urban Plan.* **2000**, *48*, 1–18. [[CrossRef](#)]
12. Kim, S.W.; Brown, R.D. Urban heat island (UHI) intensity and magnitude estimations: A systematic literature review. *Sci. Total Environ.* **2021**, *779*, 146389. [[CrossRef](#)] [[PubMed](#)]
13. Maharjan, M.; Aryal, A.; Shakya, B.M.; Talchabhadel, R.; Thapa, B.; Kumar, S. Evaluation of Urban Heat Island (UHI) Using Satellite Images in Densely Populated Cities of South Asia. *Earth* **2021**, *2*, 86–110. [[CrossRef](#)]
14. Li, H.; Zhou, Y.; Li, X.; Meng, L.; Wang, X.; Wu, S.; Sodoudi, S. A new method to quantify surface urban heat island intensity. *Sci. Total Environ.* **2018**, *624*, 262–272. [[CrossRef](#)]
15. Oh, J.W.; Ngarambe, J.; Duhirwe, P.N.; Yun, G.Y.; Santamouris, M. Using deep-learning to forecast the magnitude and characteristics of urban heat island in Seoul Korea. *Sci. Rep.* **2020**, *10*, 3559. [[CrossRef](#)] [[PubMed](#)]
16. Sun, Y.; Wang, S.; Wang, Y. Estimating local-scale urban heat island intensity using nighttime light satellite imageries. *Sustain. Cities Soc.* **2020**, *57*, 102125. [[CrossRef](#)]
17. Equere, V.; Mirzaei, P.A.; Riffat, S. Definition of a new morphological parameter to improve prediction of urban heat island. *Sustain. Cities Soc.* **2020**, *56*, 102021. [[CrossRef](#)]
18. Deilami, K.; Kamruzzaman, M.; Liu, Y. Urban heat island effect: A systematic review of spatio-temporal factors, data, methods, and mitigation measures. *Int. J. Appl. Earth Obs. Geoinf.* **2018**, *67*, 30–42. [[CrossRef](#)]
19. Shirani-Bidabadi, N.; Nasrabadi, T.; Faryadi, S.; Larijani, A.; Roodposhti, M.S. Evaluating the spatial distribution and the intensity of urban heat island using remote sensing, case study of Isfahan city in Iran. *Sustain. Cities Soc.* **2019**, *45*, 686–692. [[CrossRef](#)]
20. Howard, L. *The Climate of London Deduced from Meteorological Observations*; W. Phillips: London, UK, 1818.
21. Sultana, S.; Satyanarayana, A.N.V. Assessment of urbanisation and urban heat island intensities using landsat imageries during 2000–2018 over a sub-tropical Indian City. *Sustain. Cities Soc.* **2020**, *52*, 101846. [[CrossRef](#)]
22. Rani, M.; Kumar, P.; Pandey, P.C.; Srivastava, P.K.; Chaudhary, B.; Tomar, V.; Mandal, V.P. Multi-temporal NDVI and surface temperature analysis for Urban Heat Island inbuilt surrounding of sub-humid region: A case study of two geographical regions. *Remote Sens. Appl. Soc. Environ.* **2018**, *10*, 163–172. [[CrossRef](#)]
23. Mathew, A.; Khandelwal, S.; Kaul, N. Investigating spatial and seasonal variations of urban heat island effect over Jaipur city and its relationship with vegetation, urbanization and elevation parameters. *Sustain. Cities Soc.* **2017**, *35*, 157–177. [[CrossRef](#)]
24. Guha, S.; Govil, H.; Diwan, P. Analytical study of seasonal variability in land surface temperature with normalized difference vegetation index, normalized difference water index, normalized difference built-up index, and normalized multiband drought index. *J. Appl. Remote Sens.* **2019**, *13*, 024518. [[CrossRef](#)]
25. Yu, Q.; Acheampong, M.; Pu, R.; Landry, S.M.; Ji, W.; Dahigamuwa, T. Assessing effects of urban vegetation height on land surface temperature in the City of Tampa, Florida, USA. *Int. J. Appl. Earth Obs. Geoinf.* **2018**, *73*, 712–720. [[CrossRef](#)]
26. Sussman, H.S.; Raghavendra, A.; Zhou, L. Impacts of increased urbanization on surface temperature, vegetation, and aerosols over Bengaluru, India. *Remote Sens. Appl. Soc. Environ.* **2019**, *16*, 100261. [[CrossRef](#)]
27. Bashit, N.; Prasetyo, Y.; Sukmono, A. Analysis of Built-up Land Spatial Patterns Using Multitemporal Satellite Imagery in Pekalongan City. *J. Appl. Geospat. Inf.* **2020**, *4*, 356–362. [[CrossRef](#)]
28. Nguyen, C.; Chidthaisong, A.; Diem, P.K.; Huo, L.-Z. A modified bare soil index to identify bare land features during agricultural fallow-period in southeast Asia using Landsat 8. *Land* **2021**, *10*, 231. [[CrossRef](#)]
29. Yang, Y.; Cao, C.; Pan, X.; Li, X.; Zhu, X. Downscaling land surface temperature in an arid area by using multiple remote sensing indices with random forest regression. *Remote Sens.* **2017**, *9*, 789. [[CrossRef](#)]
30. Souza, C.M.; Shimbo, J.Z.; Rosa, M.R.; Parente, L.L.; Alencar, A.A.; Rudorff, B.F.T.; Hasenack, H.; Matsumoto, M.; Ferreira, L.G.; Souza-Filho, P.W.M.; et al. Reconstructing Three Decades of Land Use and Land Cover Changes in Brazilian Biomes with Landsat Archive and Earth Engine. *Remote Sens.* **2020**, *12*, 2735. [[CrossRef](#)]
31. BBS (Bangladesh Bureau of Statistics). *Bangladesh Household Survey*; Bangladesh Bureau of Statistics: Dhaka, Bangladesh, 2012.
32. Rahman, M.N.; Shozib, S.H. Seasonal Variability of Waterlogging in Rangpur City Corporation Using GIS and Remote Sensing Techniques. *Geosfera Indones.* **2021**, *6*, 143–156. [[CrossRef](#)]

33. Rai, R.; Zhang, Y.; Paudel, B.; Li, S.; Khanal, N.R. A Synthesis of Studies on Land Use and Land Cover Dynamics during 1930–2015 in Bangladesh. *Sustainability* **2017**, *9*, 1866. [CrossRef]
34. Rahman, M.N.; Rony, M.R.H.; Jannat, F.A. Spatiotemporal evaluation of drought trend during 1979–2019 in seven climatic zones of Bangladesh. *Heliyon* **2021**, *7*, e08249. [CrossRef] [PubMed]
35. Islam, A.R.M.T.; Islam, H.; Shahid, S.; Khatun, M.K.; Ali, M.M.; Rahman, M.; Ibrahim, S.M.; Almoajel, A.M. Spatiotemporal nexus between vegetation change and extreme climatic indices and their possible causes of change. *J. Environ. Manag.* **2021**, *289*, 112505. [CrossRef] [PubMed]
36. Dewan, A.; Kiselev, G.; Botje, D.; Mahmud, G.I.; Bhuiyan, H.; Hassan, Q.K. Surface urban heat island intensity in five major cities of Bangladesh: Patterns, drivers and trends. *Sustain. Cities Soc.* **2021**, *71*, 102926. [CrossRef]
37. Itzhak-Ben-Shalom, H.; Alpert, P.; Potchter, O.; Samuel, R. MODIS summer SUHI cross-sections anomalies over the meg-acities of the monsoon Asia region and global trends. *Open Atmos. Sci. J.* **2017**, *11*, 121–136. [CrossRef]
38. Dewan, A.; Kiselev, G.; Botje, D. Diurnal and seasonal trends and associated determinants of surface urban heat islands in large Bangladesh cities. *Appl. Geogr.* **2021**, *135*, 102533. [CrossRef]
39. Li, J.; Song, C.; Cao, L.; Zhu, F.; Meng, X.; Wu, J. Impacts of landscape structure on surface urban heat islands: A case study of Shanghai, China. *Remote Sens. Environ.* **2011**, *115*, 3249–3263. [CrossRef]
40. Talukdar, S.; Eibek, K.U.; Akhter, S.; Ziaul, S.; Islam, A.R.M.T.; Mallick, J. Modeling fragmentation probability of land-use and land-cover using the bagging, random forest and random subspace in the Teesta River Basin, Bangladesh. *Ecol. Indic.* **2021**, *126*, 107612. [CrossRef]
41. Banglapedia. Climatic. Available online: <http://en.banglapedia.org/index.php?title=Climatic> (accessed on 20 February 2021).
42. Banglapedia. Climatic Zone. Available online: http://en.banglapedia.org/index.php?title=Climatic_Zone#:~:{}:text (accessed on 23 February 2021).
43. Macrotrends. Available online: www.macrotrends.net (accessed on 25 February 2021).
44. World Bank. Climate Change Overview. Available online: <https://climateknowledgeportal.worldbank.org/country/bangladesh> (accessed on 2 December 2021).
45. Al Kafy, A.; Al-Faisal, A.; Hasan, M.M.; Sikdar, S.; Khan, M.H.H.; Rahman, M.; Islam, R. Impact of LULC Changes on LST in Rajshahi District of Bangladesh: A Remote Sensing Approach. *J. Geogr. Stud.* **2019**, *3*, 11–23. [CrossRef]
46. Al Kafy, A.; Faisal, A.A.; Rahman, S.; Islam, M.; Al Rakib, A.; Islam, A.; Khan, H.H.; Sikdar, S.; Sarker, H.S.; Mawa, J.; et al. Prediction of seasonal urban thermal field variance index using machine learning algorithms in Cumilla, Bangladesh. *Sustain. Cities Soc.* **2020**, *64*, 102542. [CrossRef]
47. El-Zeiny, A.M.; Effat, H.A. Environmental monitoring of spatiotemporal change in land use/land cover and its impact on land surface temperature in El-Fayoum governorate, Egypt. *Remote Sens. Appl. Soc. Environ.* **2017**, *8*, 266–277. [CrossRef]
48. Verma, P.; Raghunashi, A.; Srivastava, P.K. Appraisal of kappa-based metrics and disagreement indices of accuracy assessment for parametric and nonparametric techniques used in LULC classification and change detection. *Model. Earth Syst. Environ.* **2020**, *6*, 1045–1059. [CrossRef]
49. Matsushita, B.; Yang, W.; Chen, J.; Onda, Y.; Qiu, G. Sensitivity of the Enhanced Vegetation Index (EVI) and Normalized Difference Vegetation Index (NDVI) to Topographic Effects: A Case Study in High-density Cypress Forest. *Sensors* **2007**, *7*, 2636–2651. [CrossRef]
50. USGS. Landsat Normalized Difference Vegetation Index. Available online: <https://www.usgs.gov/landsat-missions/landsat-normalized-difference-vegetation-index> (accessed on 2 December 2021).
51. Fatemi, M.; Narangifard, M. Monitoring LULC changes and its impact on the LST and NDVI in District 1 of Shiraz City. *Arab. J. Geosci.* **2019**, *12*, 127. [CrossRef]
52. He, B.-J.; Zhao, Z.-Q.; Shen, L.-D.; Wang, H.-B.; Li, L.-G. An approach to examining performances of cool/hot sources in mitigating/enhancing land surface temperature under different temperature backgrounds based on landsat 8 image. *Sustain. Cities Soc.* **2018**, *44*, 416–427. [CrossRef]
53. Gutman, G.; Huang, C.; Chander, G.; Noojipady, P.; Masek, J.G. Assessment of the NASA–USGS Global Land Survey (GLS) datasets. *Remote Sens. Environ.* **2013**, *134*, 249–265. [CrossRef]
54. Weng, Q.; Lu, D.; Schubring, J. Estimation of land surface temperature–vegetation abundance relationship for urban heat island studies. *Remote Sens. Environ.* **2004**, *89*, 467–483. [CrossRef]
55. Avdan, U.; Jovanovska, G. Algorithm for Automated Mapping of Land Surface Temperature Using LANDSAT 8 Satellite Data. *J. Sens.* **2016**, *2016*, 1480307. [CrossRef]
56. Hu, Y.; Hou, M.; Jia, G.; Zhao, C.; Zhen, X.; Xu, Y. Comparison of surface and canopy urban heat islands within megacities of eastern China. *ISPRS J. Photogramm. Remote Sens.* **2019**, *156*, 160–168. [CrossRef]
57. Molla, M.H.; Chowdhury, M.A.T.; Islam, A.Z.M.Z. Spatiotemporal Change of Urban Water Bodies in Bangladesh: A Case Study of Chittagong Metropolitan City Using Remote Sensing (RS) and GIS Analytic Techniques, 1989–2015. *J. Indian Soc. Remote Sens.* **2020**, *49*, 773–792. [CrossRef]
58. Hassan, M.M.; Nazem, M.N.I. Examination of land use/land cover changes, urban growth dynamics, and environmental sustainability in Chittagong city, Bangladesh. *Environ. Dev. Sustain.* **2015**, *18*, 697–716. [CrossRef]
59. Morshed, N.; Yorke, C.; Zhang, Q. Urban Expansion Pattern and Land Use Dynamics in Dhaka, 1989–2014. *Prof. Geogr.* **2016**, *69*, 396–411. [CrossRef]

60. Hassan, M.M. Monitoring land use/land cover change, urban growth dynamics and landscape pattern analysis in five fastest urbanized cities in Bangladesh. *Remote Sens. Appl. Soc. Environ.* **2017**, *7*, 69–83. [[CrossRef](#)]
61. Congalton, R.G. A review of assessing the accuracy of classifications of remotely sensed data. *Remote Sens. Environ.* **1991**, *37*, 35–46. [[CrossRef](#)]
62. Ishtiaque, T.A.; Tasin, Z.T.; Akter, K.S. Urban heat Island intensity assessment through comparative study on land surface temperature and normalized difference vegetation index: A case study of Chittagong, Bangladesh. *Int. J. Urban Civ. Eng.* **2017**, *11*, 37–42.
63. Gazi, Y.; Rahman, Z.; Uddin, M.; Rahman, F.M.A. Spatio-temporal dynamic land cover changes and their impacts on the urban thermal environment in the Chittagong metropolitan area, Bangladesh. *GeoJournal* **2020**, *86*, 2119–2134. [[CrossRef](#)]
64. Parvin, N.S.; Abudu, D. Estimating Urban Heat Island Intensity using Remote Sensing Techniques in Dhaka City. *Int. J. Sci. Eng. Res.* **2017**, *8*, 289–298. [[CrossRef](#)]
65. Faridatul, M.I. Spatiotemporal Effects of Land Use and River Morphological Change on the Microclimate of Rajshahi Metropolitan Area. *J. Geogr. Inf. Syst.* **2017**, *09*, 466–481. [[CrossRef](#)]
66. Uddin, J.; Mondal, C. Effect of earth covering and water body on land surface temperature (LST). *J. Civ. Eng. Sci. Technol.* **2020**, *11*, 45–56. [[CrossRef](#)]
67. Al Rakib, A.; Akter, K.S.; Rahman, N.; Arpi, S.; Kafy, A. Analyzing the Pattern of Land Use Land Cover Change and its Impact on Land Surface Temperature: A Remote Sensing Approach. In *Proceedings of the 1st International Student Research Conference-2020*; Dhaka University Research Society (DURS), University of Dhaka: Dhaka, Bangladesh, 2020.
68. Yuksel, U. Examination of the air and surface temperatures in structural and green areas in the city: The case of Ankara. *Ecology* **2008**, *18*, 66–74.
69. Myhre, G.; Myhre, A. Uncertainties in Radiative Forcing due to Surface Albedo Changes Caused by Land-Use Changes. *J. Clim.* **2003**, *16*, 1511–1524. [[CrossRef](#)]
70. Gophen, M. Land-Use, Albedo and Air Temperature Changes in the Hula Valley (Israel) during 1946–2008. *Open J. Mod. Hydrol.* **2014**, *4*, 101–111. [[CrossRef](#)]
71. Argüeso, D.; Evans, J.; Fita, L.; Bormann, K.J. Temperature response to future urbanization and climate change. *Clim. Dyn.* **2013**, *42*, 2183–2199. [[CrossRef](#)]
72. Debbage, N.; Shepherd, J.M. The urban heat island effect and city contiguity. *Comput. Environ. Urban Syst.* **2015**, *54*, 181–194. [[CrossRef](#)]
73. Huang, F.; Zhan, W.; Voogt, J.; Hu, L.; Wang, Z.; Quan, J.; Guo, Z. Temporal upscaling of surface urban heat island by incorporating an annual temperature cycle model: A tale of two cities. *Remote Sens. Environ.* **2016**, *186*, 1–12. [[CrossRef](#)]
74. Kant, Y.; Azim, S.; Mitra, D. Analyzing the influence of urban growth on thermal environment through demographic, environmental, and physical parameters in Bangladesh. In *Land-Atmospheric Research Applications in South and Southeast Asia*; Springer: Cham, Switzerland, 2018; pp. 613–639.
75. Quan, J.; Zhan, W.; Chen, Y.; Wang, M.; Wang, J. Time series decomposition of remotely sensed land surface temperature and investigation of trends and seasonal variations in surface urban heat islands. *J. Geophys. Res. Atmos.* **2016**, *121*, 2638–2657. [[CrossRef](#)]
76. Wang, Y.; Berardi, U.; Akbari, H. Comparing the effects of urban heat island mitigation strategies for Toronto, Canada. *Energy Build.* **2016**, *114*, 2–19. [[CrossRef](#)]
77. Hu, X.-M.; Xue, M.; Klein, P.M.; Illston, B.G.; Chen, S. Analysis of Urban Effects in Oklahoma City using a Dense Surface Observing Network. *J. Appl. Meteorol. Clim.* **2016**, *55*, 723–741. [[CrossRef](#)]
78. Roy, S.; Pandit, S.; Eva, E.A.; Bagmar, S.H.; Papia, M.; Banik, L.; Dube, T.; Rahman, F.; Razi, M.A. Examining the nexus between land surface temperature and urban growth in Chattogram Metropolitan Area of Bangladesh using long term Landsat series data. *Urban Clim.* **2020**, *32*, 100593. [[CrossRef](#)]
79. Chakraborty, T.; Lee, X. A simplified urban-extent algorithm to characterize surface urban heat islands on a global scale and examine vegetation control on their spatiotemporal variability. *Int. J. Appl. Earth Obs. Geoinf.* **2018**, *74*, 269–280. [[CrossRef](#)]
80. Peng, J.; Hu, Y.; Dong, J.; Liu, Q.; Liu, Y. Quantifying spatial morphology and connectivity of urban heat islands in a megacity: A radius approach. *Sci. Total Environ.* **2020**, *714*, 136792. [[CrossRef](#)]
81. Li, L.; Zha, Y.; Zhang, J. Spatially non-stationary effect of underlying driving factors on surface urban heat islands in global major cities. *Int. J. Appl. Earth Obs. Geoinf.* **2020**, *90*, 102131. [[CrossRef](#)]
82. Raj, S.; Paul, S.K.; Chakraborty, A.; Kuttippurath, J. Anthropogenic forcing exacerbating the urban heat islands in India. *J. Environ. Manag.* **2020**, *257*, 110006. [[CrossRef](#)]
83. Ojeh, V.N.; Balogun, A.A.; Okhimamhe, A.A. Urban-Rural Temperature Differences in Lagos. *Climate* **2016**, *4*, 29. [[CrossRef](#)]
84. Shojaei, P.; Gheysari, M.; Myers, B.; Eslamian, S.; Shafieiyou, E.; Esmaeili, H. Effect of different land cover/use types on canopy layer air temperature in an urban area with a dry climate. *Build. Environ.* **2017**, *125*, 451–463. [[CrossRef](#)]
85. Chapman, S.; Watson, J.E.; Salazar, A.; Thatcher, M.; McAlpine, C.A. The impact of urbanization and climate change on urban temperatures: A systematic review. *Landsc. Ecol.* **2017**, *32*, 1921–1935. [[CrossRef](#)]
86. Mora, C.; Dousset, B.; Caldwell, I.R.; Powell, F.E.; Geronimo, R.C.; Bielecki, C.R.; Counsell, C.W.W.; Dietrich, B.S.; Johnston, E.T.; Louis, L.V.; et al. Global risk of deadly heat. *Nat. Clim. Chang.* **2017**, *7*, 501–506. [[CrossRef](#)]

87. Rahman, M.M.; Rahman, M.M.; Momotaz, M. Environmental quality evaluation in Dhaka City Corporation—Using satellite imagery. *Proc. Inst. Civ. Eng. Urban Des. Plan.* **2019**, *172*, 13–25. [[CrossRef](#)]
88. Chun, B.; Guldman, J.M. Impact of greening on the urban heat island: Seasonal variations and mitigation strategies. *Comput. Environ. Urban Syst.* **2018**, *71*, 165–176. [[CrossRef](#)]
89. Islam, A.R.M.T.; Ahmed, I.; Rahman, S. Trends in cooling and heating degree-days overtimes in Bangladesh? An investigation of the possible causes of changes. *Nat. Hazards* **2020**, *101*, 879–909. [[CrossRef](#)]
90. Oleson, K.W.; Bonan, G.B.; Schaaf, C.; Gao, F.; Jin, Y.; Strahler, A. Assessment of global climate model land surface albedo using MODIS data. *Geophys. Res. Lett.* **2003**, *30*. [[CrossRef](#)]